AMERICAN SOCIETY FOR MICROBIOLOGY | mSystems

Host-Microbial Interactions | Research Article

Multi-omics analysis reveals the interplay between intratumoral bacteria and glioma

Ting Li,[1,2] Zhanyi Zhao,[1,2] Meichang Peng,[1,2] Lu Zhang,[1,2] Cheng Wang,[1,2] Feiyang Luo,[1] Meiqin Zeng,[1,2] Kaijian Sun,[1,2] Zhencheng Fang,[1] Yunhao Luo,[1] Yugu Xie,[1] Cui Lv,[1] Jiaxuan Wang,[1] Jian-Dong Huang,[1,3,4,5,6] Hongwei Zhou,[1] Haitao Sun[1,2,7]

AUTHOR AFFILIATIONS See affiliation list on p. 22.

ABSTRACT Emerging evidence highlights the potential impact of intratumoral microbiota on cancer. However, the microbial composition and function in glioma remains elusive. Consequently, our study aimed to investigate the microbial community composition in glioma tissues and elucidate its role in glioma development. We parallelly performed microbial profiling, transcriptome sequencing, and metabolomics detection on tumor and adjacent normal brain tissues obtained from 50 glioma patients. We employed immunohistochemistry, multicolor immunofluorescence, and fluorescence *in situ* hybridization (FISH) staining to observe the presence and location of bacteria. Furthermore, an animal model was employed to validate the impact of key bacteria on glioma development. Six genera were found to be significantly enriched in glioma tissues compared to adjacent normal brain tissues, including *Fusobacterium*, *Longibaculum*, *Intestinimonas*, *Pasteurella*, *Limosilactobacillus,* and *Arthrobacter*. Both bacterial RNA and lipopolysaccharides (LPS) were observed in glioma tissues. Integrated microbiomics, transcriptomics, and metabolomics revealed that genes associated with intratumoral microbes were enriched in multiple synapse-associated pathways and that metabolites associated with intratumoral microbes were (R)-*N*-methylsalsolinol, *N*-acetylaspartylglutamic acid, and *N*-acetyl-L-aspartic acid. Further mediation analysis suggested that the intratumoral microbiome may affect the expression of neuron-related genes through bacteria-associated metabolites. In addition, both *in vivo* and *in vitro* models of glioma show that *Fusobacterium nucleatum* promotes glioma proliferation and upregulates CCL2, CXCL1, and CXCL2 levels. Our findings shed light on the intricate interplay between intratumoral bacteria and glioma.

IMPORTANCE Our study adopted a multi-omics approach to unravel the impact of intratumoral microbes on neuron-related gene expression through bacteria-associated metabolites. Importantly, we found bacterial RNA and LPS signals within glioma tissues, which were traditionally considered sterile. We identified key microbiota within glioma tissues, including *Fusobacterium nucleatum* (Fn). Through *in vivo* and *in vitro* experiments, we identified the crucial role of Fn in promoting glioma progression, suggesting that Fn could be a potential diagnostic and therapeutic target for glioma patients. These findings offer valuable insights into the intricate interplay between intratumoral bacteria and glioma, offering novel inspiration to the realm of glioma biology.

KEYWORDS glioma, intratumoral microbiota, metabolomics, multi-omics, *Fusobacterium nucleatum*

Glioma, as the predominant primary malignancy of the central nervous system (1), poses a formidable challenge for treatment worldwide owing to its high recurrence, mortality, and poor prognosis. It is imperative to further elucidate the pathogenic mechanisms of glioma and develop novel therapeutic strategies. Increasing evidence

Editor Emily K. Cope, Northern Arizona University, Flagstaff, Arizona, USA

Address correspondence to Haitao Sun, 2009sht@smu.edu.cn.

Ting Li and Zhanyi Zhao contributed equally to this article. Author order was determined both alphabetically and in order of increasing seniority.

The authors declare no conflict of interest.

See the funding table on p. 23.

Received 28 March 2024
Accepted 29 October 2024
Published 11 December 2024

has underscored the significant contributions made by intratumoral microbiota in tumor progression (2), metastasis (3), and treatment (4). Therefore, elucidating the molecular characteristics of glioma from the perspective of the intratumoral microbiome is of great significance for understanding the etiology of glioma and developing new bacteria-based therapeutic strategies.

Whether microbiota exists in glioma, or even in the brain remains issues under debate. The brain has traditionally been regarded as a sterile organ due to the blood-brain barrier. However, recent evidence indicates that microbiota may directly inhabit the brain under non-inflammatory and non-traumatic conditions (5). Gram-negative bacterial molecules and *Porphyromonas gingivalis* were detected in the brains of Alzheimer's disease patients and found to be associated with tau protein accumulation (6–8). Rombert et al. (8) reported in an abstract at the American Neuroscience Annual Meeting that they found rod-shaped bacteria in the healthy human post-mortem brains under electron microscopy.

In addition, a study conducted a comprehensive detection and analysis of the intratumoral microbiota of seven types of solid tumors, including glioblastoma (9). They found that glioblastoma harbored a unique microbial community and that the level of bacterial DNA was not low. Due to the small sample size and the limitations of the experimental design, this study did not reveal the role of intratumoral microbiota in glioblastoma.

In our previous work (10), we used intact tissues and combined tissue clearing, immunofluorescence staining methods to observe bacterial lipopolysaccharides (LPS) in glioma in three-dimensional space. Although we further confirmed the presence of bacterial LPS in human glioma tissue morphologically, more evidence is needed to elucidate the spatial relationship and function of bacteria in glioma.

The study of the tumor microbiome is a challenging task due to the low intratumor bacterial biomass and uncultivability of some microbial species. Novel high-resolution techniques are urgently required to facilitate further research. Multi-omics techniques can elucidate tumor microbiota at different levels, thereby facilitating a comprehensive understanding of the intricate biological processes associated with tumor microbiota.

To this end, we simultaneously performed 16S rRNA sequencing, metabolomics and transcriptomics analyses on glioma tissue (G) samples, and adjacent normal brain tissue (NAT) samples. Our results suggested that intratumoral microbiota of glioma may affect the expression of neuron-related genes through bacteria-associated metabolites.

MATERIALS AND METHODS

Human subjects and sample collection

We obtained 110 fresh frozen tissues, 8 paraffin tissues, and 10 stool samples from patients with pathologically confirmed glioma. The clinical information of the patients was shown in Table S1. The stool samples were taken before cancer treatment, and individuals who received preoperative radiation or chemotherapy treatment or had a previous history of glioma were excluded. All samples were collected from Zhujiang Hospital of Southern Medical University (Guangzhou, China).

Tissue samples were meticulously collected in sterile cryotubes and promptly transported using a portable liquid nitrogen tank to the Clinical Biobank Center, where they were kept at −196°C for long-term storage until DNA extraction. Fecal samples are rapidly transferred to a −80°C freezer for storage until further use.

Mice

Athymic BALB/c nude mice (4 weeks; 20–25 g) were purchased from GemPharmatech Corporation (Nanjing, China) and maintained in a specific pathogen-free environment under a 12 h light-dark cycle with free access to food and water.

Cell lines and culture

Human glioblastoma lines (U87, U251, and Ln229) were obtained from the Chinese Academy of Sciences. The cells were cultured in Dulbecco's Modified Eagle Medium (DMEM; Gibco, Carlsbad, CA, USA) supplemented with 10% fetal bovine serum (Gibco). All cell lines were at 37°C and 5% CO2 in a humid environment.

Bacterial strains

Fusobacterium nucleatum ATCC 25586 (Fn) was gifted kindly by Dr. Songhe Guo. Fn was grown anaerobically at 37°C for 48–72 h in blood agar plate (Oxoid, UK). Fn were centrifuged and then suspended to a concentration of 1×10^6 colony-forming units (CFUs)/mL with PBS for subsequent experiments.

Isolation and culture of human-derived organoids

We performed primary isolation of organoids using fresh tumor samples obtained from glioblastoma patients post-surgery. Fresh glioblastoma tissues were rinsed twice with a washing solution and then minced. The tissues were digested with a digestive solution at 37°C. After digestion, the sample was centrifuged, the supernatant was discarded, and the cells were resuspended in Hanks' balanced salt solution (HBSS) and passed through a 100 µm cell strainer. The resulting cell filtrate was centrifuged again, and the supernatant was discarded. The cell pellet was treated with erythrocyte lysis buffer for 10 min. After centrifugation and removal of the supernatant, the cells were resuspended in a medium containing growth factors and matrix gel and seeded into low-adhesion 6-well plates (Corning). Finally, the plates were placed in a 37°C incubator on a shaker for culture.

Cell counting kit-8 (CCK-8) assays

Glioma cells were seeded in 96-well plates at 2,000 cells per well in the growth medium. Cells were untreated or with Fn at a multiplicity of infection (MOI) of 50:1. At 0 h (when the cells adhered), and at 24, 48, 72, and 96 h, 10 µL of CCK-8 reagent (APEXbio) was added to each well, followed by gentle mixing. The plates were then incubated in the dark for 2 h at 37°C. The absorbance at 450 nm was measured using a full-wavelength microplate reader (THERMO Scientific, Multiskan Sky).

Colony formation assays

Glioma cells were seeded in 6-well plates at 800 cells per well. Cells were untreated or with Fn at a multiplicity of infection (MOI) of 50:1 and cultured for 10 days. Subsequently, the culture medium was removed, and the cell colonies were fixed with 4% paraformaldehyde (Biosharp) for 10 min at 25°C, followed by staining with 0.1% crystal violet (BKMAMLAB) for 20 min. Images were taken, and the colonies were counted using ImageJ software.

Measurement of organoid diameter

After resuscitating the organoids, the cryopreservative solution was removed by centrifugation, and the cell pellet was resuspended in antibiotic-free organoid medium. Glioma organoids were inoculated into 24-well plates at 40,000 cells/well, either untreated or incubated with bacteria at an MOI of 50:1. After 2 days of culture and formation, each organoid was photographed using a Nikon Ts2FL inverted microscope at 4× magnification for each well. Subsequent images were taken every 24 h. The diameters of the organoids were then measured from the photographs using ImageJ.

Organoid embedding, sectioning, HE staining, and immunofluorescence

On the 5th day of co-culture, after imaging, organoids were collected and fixed with 1 mL of 4% paraformaldehyde for 1 h. They were then transferred to 1.5 mL centrifuge tubes,

and 20–50 µL of molten agarose was added to the organoid pellet and placed on ice for 30 min to solidify. The organoids were dehydrated according to the tissue processor protocol and embedded in paraffin the next day. Paraffin blocks were sectioned continuously into 8 µm sections using a microtome. The prepared organoid sections were collected, and HE staining and immunofluorescence were performed by Huayin Medical Laboratory Center. Sections of organoids were examined using a Nikon Eclipse Ti2-E inverted fluorescence microscope at 20× magnification, and images were captured in the DAPI, FITC, and TEXRED channels, respectively.

ATP assay for organoid viability

Passaged glioblastoma organoids were seeded into low-adhesion 96-well plates (Corning) at 10,000 cells/well. The organoids were either left untreated or incubated with bacteria at an MOI of 50:1 and cultured on a shaker in a 37°C incubator. Two blank control groups without organoids were also set up. At 0, 24, 48, 72, and 96 h, the ATP levels were measured using an ATP assay kit (abs50059, Absin) according to the manufacturer's instructions.

ELISA detection

A 50 µg tumor tissue sample was homogenized using a tissue grinder (LUKA, LUKYM II) and then centrifuged to collect the supernatant. For U87 cells and organoids, they were sonicated at a specific power setting and subjected to repeated freeze-thaw cycles at −20°C and room temperature to obtain the supernatant. According to the manufacturer's protocol (Jiangsu Jingmei Biological Technology Co., Ltd.), 10 µL of each sample and 40 µL of sample diluent were added to a 96-well plate for ELISA analysis. Finally, the absorbance at 450 nm was measured for each well.

Multiplex immunofluorescent assay

Four-micromolar paraffin sections were deparaffinized in xylene and rehydrated in a series of graded alcohols. Antigen extraction was performed in citrate buffer (pH 6), boiled at high power in a microwave oven for 20 s, maintained at low power for 5 min at low boiling state, and cooled naturally after turning off the heat. Multiplex fluorescence labeling was performed using Tyramide signal amplification-dendron-fluorophores with NEON 7-color Allround Discovery Kit for FFPE (Histova Biotechnology). Multiplex antibody panels applied in this study are CD68 (abcam#213363, 1:200), GFAP (abcam#68428, 1:200), LPS (Lipopolysaccharide Core, HycultBiotech#HM6011, 1:200), DAPI (abcam#ab104139). After detecting all antibodies, images were taken using TissueFAXS imaging software (v7.134) and viewed with TissueFAXS Viewer software, and fluorescent positive cells were counted using StrataQuest tissue flow cytometry quantitative analysis system. For detailed analytical methods, please see the Supplemental Methods.

Immunohistochemistry

The pretreatment of paraffin tissue sections was performed according to the steps of multicolor immunofluorescence. The primary antibodies used are LPS (HycultBiotech#HM6011,1:1,000) and LTA (GeneTex#16470,1:1,000). The dyes used are DAB kits (Servicebio#G1211). Slides were scanned with Pannoramic Scan II (3D HISTECH), and images were generated with SlideViewer (v2.5, 3D HISTECH).

16S rRNA FISH

The 4 µm FFPE tissue slides were routinely deparaffinized and hydrated. Slides were stained for bacterial 16S rRNA (Cy3-labeled EUB338 probes, Future Biotech #FBFPC001) or negative control (Cy3-labeled nonspecific complement probe, Future Biotech #FBFPC001) using the direct fluorescent bacteria *in situ* hybridization detection

kit (Future Biotech #FB0016) according to the manufacturer's instructions. Slides were scanned with Pannoramic Scan II (3D HISTECH), and images were generated with SlideViewer (v2.5, 3D HISTECH).

DNA extraction and sequencing

Microbial DNA was extracted from tissue samples using the QIAGEN DNeasy PowerSoil Kit (#47014) according to manufacturer's protocol. Library construction and sequencing were performed by Novogene Corporation (Beijing, China). The downstream data processing was performed using EasyAmplicon (v1.12), VSEARCH (v2.15.2), and USEARCH (v10.0.240). For detailed analytical methods, please see the Supplemental Methods.

Microbiome data analysis

The vegan package (v2.5–6) in R (v4.1) was performed for alpha diversity analysis. The unweighted UniFrac distance matrix was generated by USEARCH. Beta diversity was calculated using principal coordinate analysis (PCoA). To visualize the results of diversity analysis, the R software package ggplot2 was used. The compositions of the microbial community in two groups were presented as stacked bar plots at the phylum levels. Analysis of variance was performed with the software package STAMP (v 2.1.3) using the storey false-discovery rate approach for the correction of *P* values. LEfSe was performed using an online utility (http://www.ehbio.com/ImageGP/index.php/Home/Index/LEFSe.html) to analyze the differences of bacterial abundance at different bacterial classification levels. Finally, Phylogenetic Investigation of Communities by Reconstruction of Unobserved States (PICRUSt) was used to predict microbial functional signatures. In the PICRUSt analysis, the significant KEGG pathways (level 3) among species were analyzed via Welch's *t*-test in STAMP using the Bonferroni correction. Statistical analysis was conducted with Graghpad Prism (v8.3) software.

Contamination correction

To prevent a false-positive rate, 15 negative controls, including 5 environmental controls, 5 DNA extraction controls, and 5 PCR controls, were prepared and sequenced alongside the tissue samples. In order to correct for contamination, binomial tests were conducted between samples and negative controls to determine their abundance. In negative control samples, the frequency of occurrence of a taxon was used to estimate p of a binomial distribution. For the binomial test, x and n represent the number of occurrences and totals, respectively. In the following analysis, those taxa with a *P*-value of 0.05 were kept.

mRNA-seq

Frozen human glioma tissues, adjacent normal brain tissue, and mouse tumor tissues were used for RNA extraction. A profiler service provided by Genergy Biotechnology Corporation (Shanghai, China) was used for RNA-seq. DESeq2 Bioconductor package was used to identify differentially expressed genes (DEGs), and remarkable DEGs were selected based on $P < 0.05$, FDR < 0.05, and a log2 (fold change) >1. The DEGs were also submitted for Kyoto Encyclopedia of Genes and Genomes (KEGG) analysis, and significant pathways with $P < 0.05$ were shown. For detailed analytical methods, please see the Supplemental Methods.

Metabolomics

Frozen human glioma tissues, adjacent normal brain tissue, and mouse tumor tissues were used for metabolomic profiling. Untargeted metabolomics profiling was performed by Biotree Biotechnology Corporation (Shanghai, China). All data were analyzed by LC-MS/MS on the UHPLC system. The differential metabolites were screened by combining the results of the student's *t*-test ($P < 0.05$) and the Variable Importance

in the Projection (VIP > 1) of the first principal component of the OPLS-DA model. Using the Kyoto Encyclopedia of Genes and Genomes (KEGG) Pathway database, we performed KEGG annotation of differential metabolites. By mapping the differential metabolites to authoritative databases such as KEGG, PubChem, The Human Metabolome Database (HMDB), after obtaining the matching information of the differential metabolites, we searched the human pathway databases and analyzed the metabolic pathways. For detailed analytical methods, please see the Supplemental Methods.

Multi-omics analyses

Correlation analysis of differentially expressed genes, differential metabolites, and differential bacteria was performed, calculating the Spearman correlation coefficient using package psych in R. Subsequently, we constructed a network integrating the interactions among differentially expressed genes, metabolites, and bacteria and visualized it using Cytoscape software. Mediation analysis was carried out using the mediation package.

Animal experiments

Xenograft mouse models were generated by subcutaneous injection of U87-MG cells (a human glioblastoma cell line) into nude mice. U87 cells (1×10^6) in the logarithmic growth phase in 100 µL of phosphate-buffered saline (PBS) were subcutaneously injected into the right flank of the mice. When the tumor volume reached 200 mm^3 (day 1), mice were randomly divided into four treatment groups (intratumoral injection): PBS group received injection of PBS, Fn group received injection of the 5×10^6 CFU *Fusobacterium nucleatum* (Fn), Fn+ metronidazole (MTZ) group received injection of Fn and MTZ treatment in addition, and MTZ group received injection of MTZ alone. For the Fn group and Fn+MTZ group, the bacteria were initially injected with PBS or metronidazole for 30 minutes before inoculation. On days 2 and 3, treat with metronidazole or a PBS vehicle twice daily, at least 8 h apart. on days 4–7, once a day. On day 8, tumor tissue was obtained and weighed. Tumor tissue was immediately frozen in liquid nitrogen for subsequent experiments.

RESULTS

Study design

To investigate tumor-associated microbial communities, we enrolled 50 glioma patients in this study. Fifty glioma and 15 matched adjacent normal brain fresh frozen tissues were used for 16S rRNA gene sequencing. We simultaneously collected 15 negative control samples, including 5 environmental controls, 5 DNA extraction controls, and 5 PCR controls for contamination filtering. Twenty glioma and six matched adjacent normal brain fresh frozen tissues were used for untargeted metabolomics analysis. Sixteen glioma and three matched adjacent normal brain fresh frozen tissues were used for transcriptomics sequencing. Four glioma and four adjacent normal brain paraffin tissues were used for bacterial imaging. To further elucidate the role of *Fusobacterium nucleatum*, the most renowned tumor-associated species within the *Fusobacterium* genus, we designed an *in vivo* animal model experiment. A schematic diagram of the design of the entire study was shown in Fig. 1.

Profiling of microbiota in human glioma tissues

To determine the homogeneity of the microbiota within glioma tissues, we conducted a survey of microbial diversity in 35 unmatched tissues and 15 matched tissues and found no significant difference in α and β diversity between the two groups. Therefore, in the subsequent analysis, we selected 50 glioma samples as representatives of the glioma group (see Fig. S1a and b in the supplemental material).

In our present microbiome investigation, overall alpha diversity of the G group was significantly higher than that of the NAT group (Fig. 2a). Employing the unconstrained

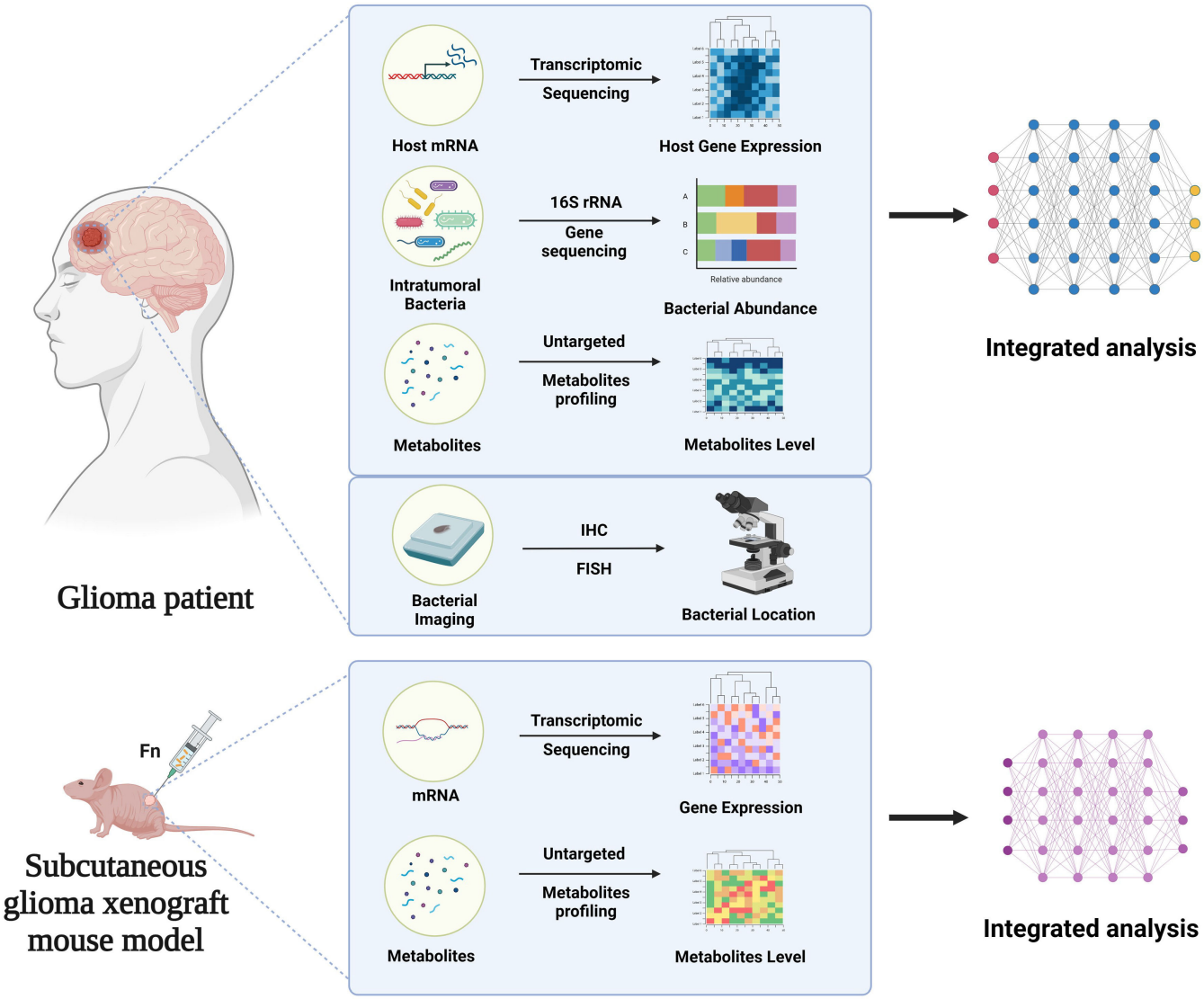

FIG 1 Schematic of research design.

principal coordinate analysis (PCoA) with Bray-Curtis distance analysis, we demonstrated a separation between the glioma-associated microbiota and those present in adjacent normal brain tissue (Fig. 2b). The results showed the microbial composition between G and NAT was markedly different. Specifically, we found that at the phylum level, the tumor-associated microbiota was dominated by *Firmicutes* and *Proteobacteria*, followed by *Actinobacteria*, *Fusobacteria,* and *Bacteroidetes* (Fig. 2c). The relative abundance of the phyla *Firmicutes* and *Fusobacteria* was greater in the G group than in the NAT group, whereas the *Proteobacteria* phylum exhibited an inverse relationship (Fig. 2d). These observations align with previous reports on investigations of the potential brain microbiome in Alzheimer's disease (11).

We performed linear discriminant effect size analysis (LEfSe) to identify potential glioma biomarkers in the intratumoral microbiota. We found 50 discriminatory OTUs as key discriminants, including six genera such as *Fusobacterium, Longibaculum*, *Intestinimonas*, *Pasteurella*, *Limosilactobacillus,* and *Arthrobacter* (all with LDA scores (log10) >4) (Fig. 2e). These genera were significantly enriched in the G group.

To characterize functional alterations in intratumoral bacteria, we used PICRUSt to predict functional orthologs between the G and NAT groups based on the Kyoto Encyclopedia of Genes and Genomes (KEGG). Following Bonferroni correction, we found

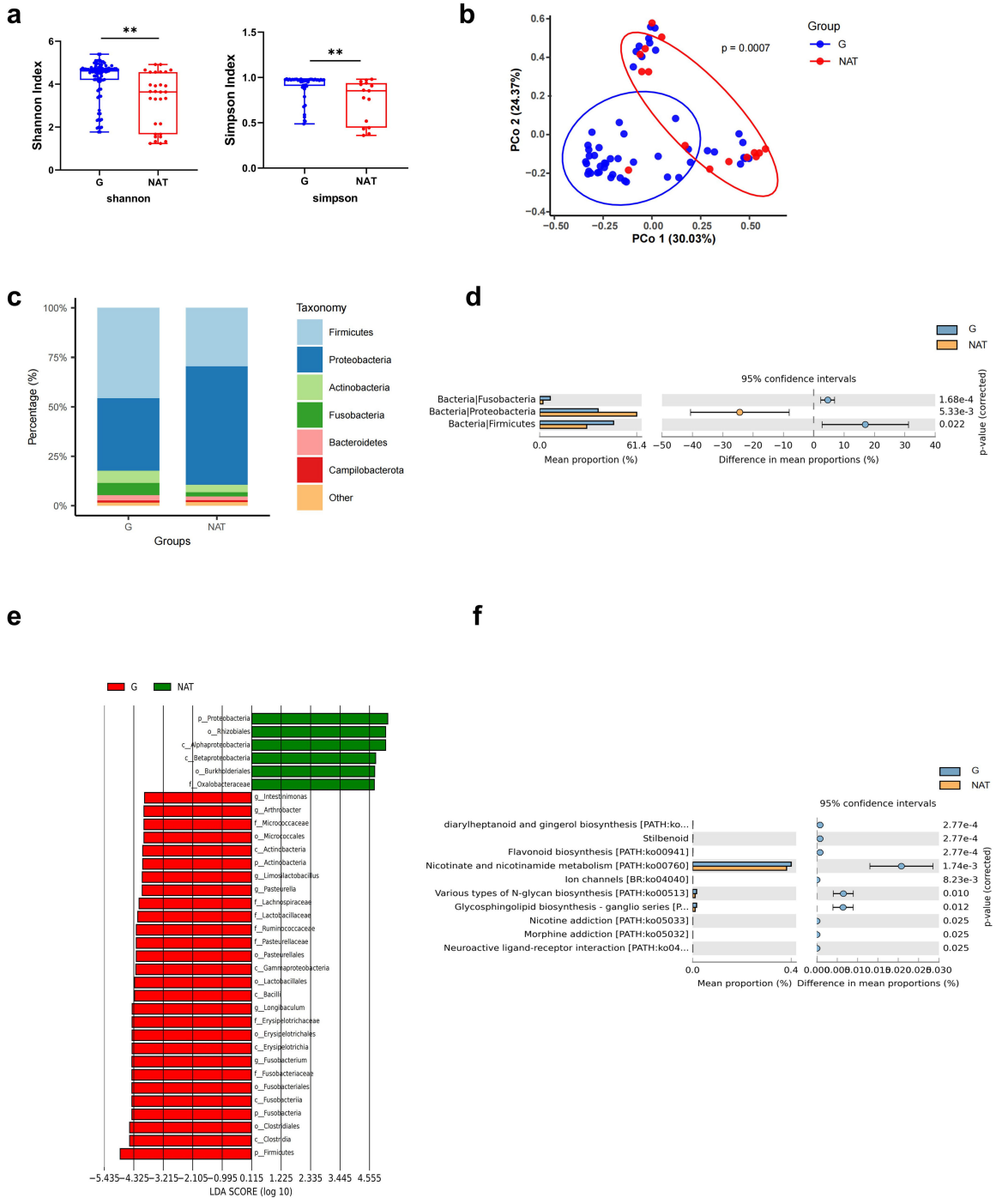

FIG 2 Profiling of tumor associated microbiota in human glioma tissue. (a) Species diversity differences between the G and NAT groups were estimated by the Shannon, and Simpson indices. *P < 0.05; **P < 0.01; NS, not significant. (b) PCoA was shown along the first two principal coordinates of Bray-Curtis distances for G and NAT. The P value was calculated by PERMANOVA. G group (blue dots); NAT group (red dots), where dots represent individual samples. (c) Microbiome community structure at the phylum levels compared in G and NAT. (d) Welch's t-test results for evaluating the relative abundance of significantly different microbiota at the phylum level. G (blue) and NAT (yellow) groups for bars and dots. (e) The distribution bar diagram based on the LEfSe analysis (LDA score (log 10)> 4) in G and NAT. (f) Enrichment pathways for prediction of microbial function between G and NAT groups based on PICRUSt analysis. G, glioma tissue; NAT, adjacent normal brain tissue.

10 pathways enriched between G group and NAT group, including neuroactive ligand-receptor interaction (Fig. 2f).

To assess potential contributing factors to microbial diversity, we conducted stratification analysis by clinical features, including age, sex, tumor size, WHO grade, and Ki-67. Interestingly, no significant relationship was observed between alpha diversity and these clinical characteristics (see Fig. S2a through e in the supplemental material); however, beta diversity was found to be significantly associated with WHO grade of glioma and Ki-67 expression (see Fig. S2f and g).

Additionally, to explore the relationship between intratumoral microbiota and gut microbiota, we collected fecal samples from the same cohort of patients and performed 16S rRNA sequencing. Strikingly, we discovered significant differences in β diversity between tumor tissue and fecal samples from glioma patients. Conversely, the differences in α diversity were not found to be significant (see Fig. S3a and b in the supplemental material).

Morphological characteristics of bacteria in human glioma tissues

To further validate the existence of bacteria in glioma tissues, we employed serial sections for immunohistochemical staining of bacterial lipoteichoic acid (LTA) and lipopolysaccharide (LPS), as well as FISH staining for 16S rRNA. Remarkably, we observed the presence of bacterial LPS and RNA signals at the same location, whereas LTA signal was not detected (Fig. 3a). Subsequently, to determine the localization of bacteria in glioma tissue, we quantified the cells co-expressing GFAP and LPS, as well as CD68 and LPS, using multicolor immunofluorescence staining on tissue sections. Statistical analysis revealed a significantly higher abundance of $GFAP^+LPS^+$ cells compared to $CD68^+LPS^+$ cells in glioma tissues (Fig. 3b). This observation suggests that bacterial LPS is more prevalent in tumor cells than macrophages. Additionally, we performed simultaneous multicolor immunofluorescence on adjacent normal brain tissue, revealing a lower bacterial LPS signal compared to glioma tissue (see Fig. S4a and b in the supplemental material).

Profiling of microbiota-associated host gene expression in human glioma tissues

To understand the potential interactions between intratumoral microbiota and host differential gene expression, we conducted transcriptome sequencing on the same set of samples and assessed their associations using Spearman correlation analysis. First, principal component analysis (PCA) revealed a significant separation between G and NAT groups (see Fig. S5a in the supplemental material). Furthermore, we observed remarkable alterations in the abundance of various mRNAs within glioma tissues compared to adjacent normal brain tissues (see Fig. S5b). According to our definition, we identified 594 differentially expressed genes (see Table S2). The KEGG pathway enrichment analysis was performed to analyze these two groups of differentially expressed genes. Figure S5c shows the top 30 enriched terms, including neuroactive ligand-receptor interaction and glioma.

Next, we performed spearman analysis to investigate the potential relationships between all the differentially expressed genes and alpha diversity. Intriguingly, we identified 52 differentially expressed genes that exhibited significant correlations with alpha diversity (Fig. 4a). Building upon these findings, we further explored the association between these 52 differentially expressed genes and 6 differential bacteria. Notably, our results revealed that 28 of these differentially expressed genes displayed a predominantly negative correlation with differential bacteria (Fig. 4b). Importantly, these 28 differentially expressed genes belong to the downregulated genes in glioma, and KEGG pathway enrichment analysis demonstrated their enrichment in pathways such as cholinergic synapse, serotonergic synapse, glutamatergic synapse, and dopaminergic synapse (Fig. 4c). To summarize, we found that these differentially expressed genes related to differential bacteria in glioma are enriched in several pathways related to

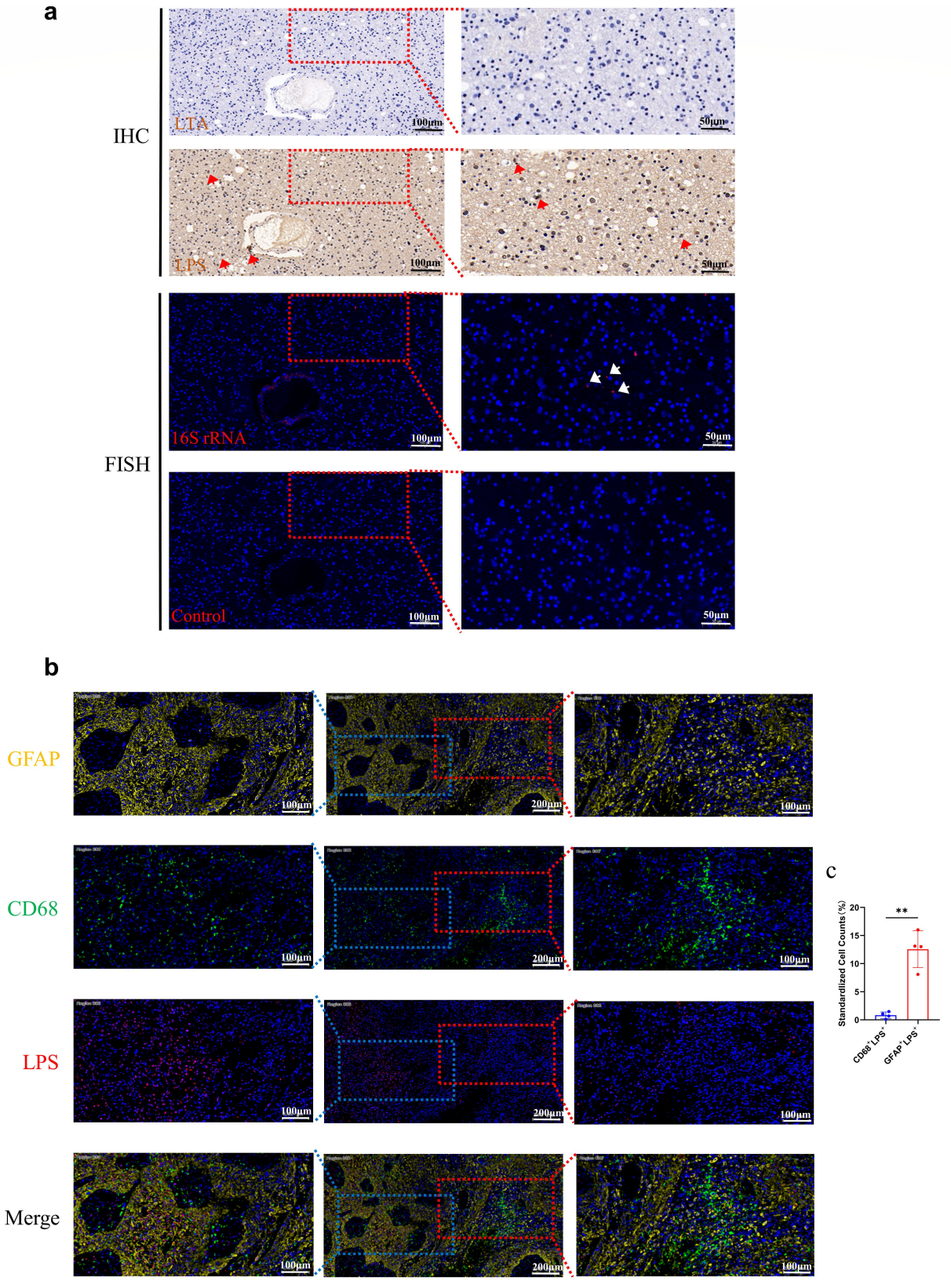

FIG 3 Morphological characteristics of bacteria in human glioma tissue. (a) Serial paraffin sections of human glioma samples were stained for bacterial LPS and LTA immunohistochemical staining, and bacterial 16S rRNA FISH staining, where the Control group used a negative probe without 16S rRNA. The left column is the image taken by 20× lens, scale bar = 100 μm. The right column is the 40× magnified image of the framed area, scale bar = 50 μm. LPS expression and

(Continued on next page)

Fig 3 (Continued)

16S rRNA FISH signal are positive at the locations marked by red and white arrows, respectively. (b) Human glioma tissue samples were stained with multicolor immunofluorescence. GFAP (yellow), CD68 (green), LPS (red), and DAPI (blue) labeled tumor cells, macrophages, bacteria, and nuclei, respectively. The middle column displays 10× images with scale bar of 200 µm. The leftmost and rightmost columns show 20× images of the tumor cell and macrophage cluster areas, respectively, framed in the 10× images. Scale bar for 20× images is 100 µm. (c) Statistics results of cell counts of GFAP + LPS double-positive cells and CD68 + LPS double-positive cells after immunofluorescence staining experiments followed by panoramic scanning. $n = 4$; $^{**}P < 0.01$.

synapses, suggesting a potential interaction between intratumoral bacteria and host, which may be associated with synaptic activity.

Profiling of microbiota-associated metabolites in human glioma tissues

We conducted metabolomic assays on the same set of glioma tissues and identified microbe-associated metabolites with microbiomic data. Remarkably, the PCA plots demonstrated a clear separation of the metabolome between G and NAT groups, both in ES + (electrospray ionization positive mode in mass spectrometry) and ES (electrospray ionization negative mode in mass spectrometry) (see Fig. S6a and b in the supplemental material). Furthermore, the OPLS-DA score scatterplots exhibited superior disjunction between the G and NAT groups, further confirming the distinct metabolic profiles of glioma tissues compared to adjacent normal tissue controls, in both ES+ and ES− (Fig. 5a and b).

To identify differential metabolites, the first principal component of variable importance in the projection (VIP) of the OPLS-DA model was obtained. We identified metabolites with VIP >1 and $P < 0.05$ as differential metabolites. We identified 79 differential metabolites in ES+ and 44 differential metabolites in ES− (see Table S3 in the supplemental material), which were visualized with a hierarchical clustering heatmap (see Fig. S6c and d). Subsequently, all the differential metabolites underwent regulatory pathway analysis to identify the metabolic pathways that were highly correlated with the metabolites. Our analysis revealed six significantly abnormal metabolic pathways in G group, including aminoacyl-tRNA biosynthesis, arginine and proline metabolism, nitrogen metabolism, taurine and hypotaurine metabolism, alanine, aspartate and glutamate metabolism, and pyrimidine metabolism. (Fig. 5c and d).

To further unravel the metabolites associated with the intratumoral microbiota in glioma, we performed a spearman analysis between all the differential metabolites and alpha diversity. Remarkably, we identified 16 metabolites that exhibited correlations with alpha diversity (Fig. 5e). Subsequently, we explored the associations between these 16 differential metabolites and six differential bacteria. Our results showed some interesting correlations: (R)-*N*-methylsalsolinol displayed positive correlations with *Longibaculum*, *Limosilactobacillus,* and *Intestinimonas*, while *N*-acetylglutamic acid, *N*-acetyl-L-aspartic acid, *N*-acetylaspartylglutamic acid, and D-alanine exhibited negative correlations with *Arthrobacter* (Fig. 5f). It is worth noting that (R)-*N*-methylsalsolinol, a dopaminergic neurotoxin, has been found to increase in cerebrospinal fluid of Parkinson's disease (12). *N*-acetylaspartylglutamic acid (NAAG) and N-acetyl-L-aspartic acid (NAA), known as neurotransmitters and their precursor substances, have been reported to inhibit the differentiation of glioma stem cells (13). Additionally, D-Alanine, a peptidoglycan constituent in bacterial cell walls, has implications as a biomarker and treatment for schizophrenia (14).

Integrated multi-omics analysis of human glioma tissues

As demonstrated in the previous sections, we have identified significant correlations between multiple genes, metabolites, and the microbiota within glioma. In this section, we further explored the complex interactions among these three factors. Network analysis unveiled a meaningful correlation, forming interconnected networks between intratumoral microbiota, tissue metabolites, and host genes (Fig. 6a and c). To assess whether genes mediate microbial effects on tumor metabolism, we performed a mediation analysis. Remarkably, we found that 5-hydroxytryptamine receptor 1D

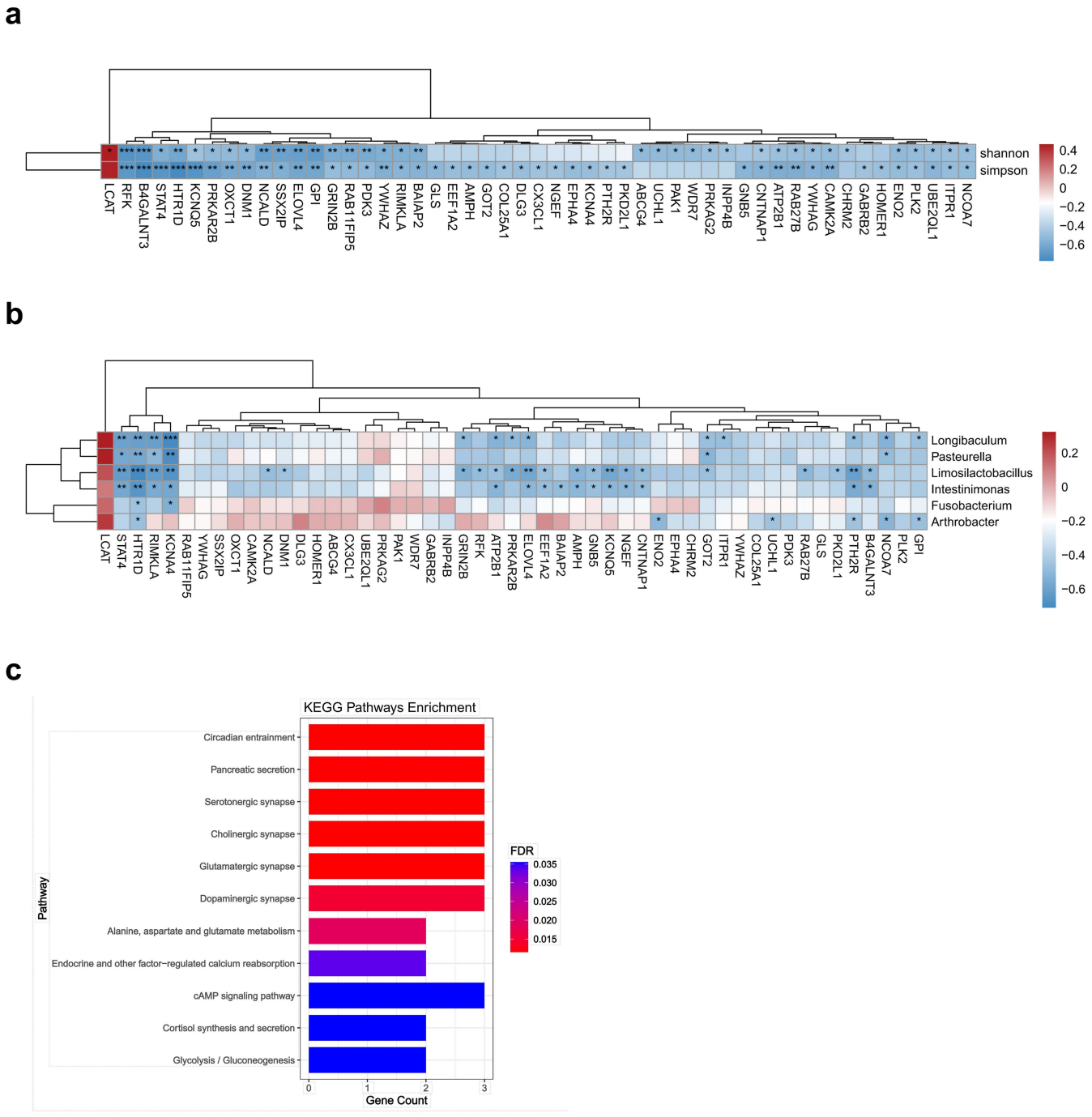

FIG 4 Gene expression associated with intratumoral microbiota in human glioma tissue. (a) Heatmap of Spearman correlation analysis between intratumoral microbiota alpha diversity and host gene expression. (b) Heatmap of Spearman correlation analysis between six differential bacteria abundance and host gene expression, red and blue indicate positive and negative correlations, respectively. *$P < 0.05$; **$P < 0.01$; ***$P < 0.001$. (c) Bar diagram of KEGG pathway enrichment analysis of 28 differentially expressed genes associated with 6 differential bacterial abundance.

(HTR1D) and signal transducer and activator of transcription 4 (STAT4) are associated with a majority of the characteristic bacteria and differential metabolites (Fig. 6b). However, the mediation effects of the 10 pathways mediated by HTR1D and STAT4 were not statistically significant ($P_{mediation} > 0.05$) (see Fig. S7a and b in the supplemental material). Further investigation focused on evaluating the function of metabolites in mediating the impact of microbiota on host gene expression. Our results indicated that

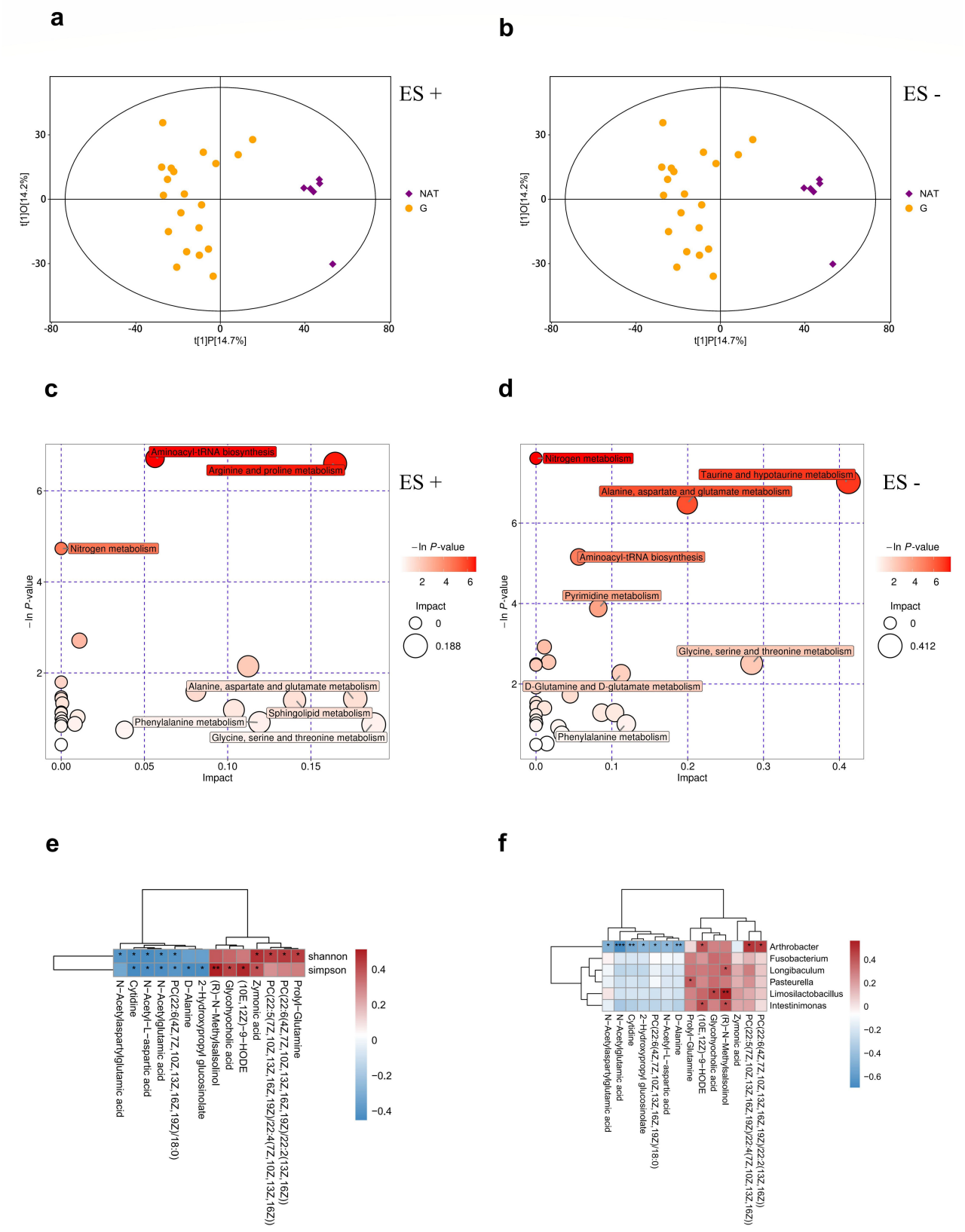

FIG 5 Profiling of tumor-associated metabolites in human glioma tissue. (a and b) Score scatter plot of OPLS-DA model between G and NAT groups. (c and d) Metabolic pathway analysis of differential metabolites between G and NAT groups. (e) Heatmap of Spearman correlation analysis between the differential metabolites and alpha diversity. (f) Heatmap of Spearman correlation analysis between the differential bacteria and metabolites, red and blue indicate positive and negative correlations, respectively. *$P < 0.05$; **$P < 0.01$; **$P < 0.001$.

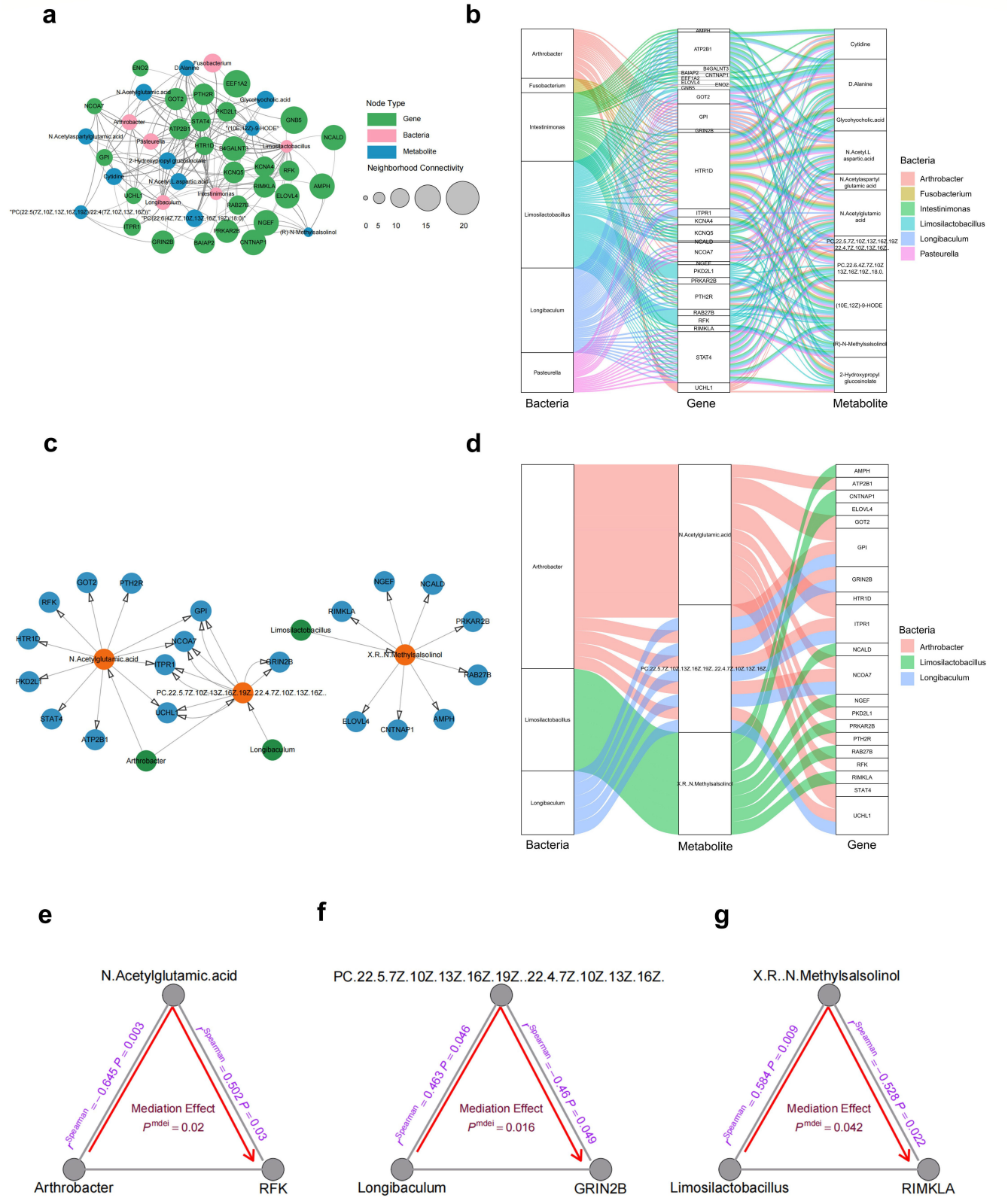

FIG 6 Integrated multi-omics analysis of human glioma tissues. (a) Network mapping of all differential metabolites and differential bacteria associated with differentially expressed genes in gene association analysis. (b) A Sankey diagram of multi-omics networks in glioma. (c) Network mapping of all differentially expressed genes (blue circles) and differential bacteria (green circles) associated with differential metabolites (orange circles) in metabolite association

(Continued on next page)

Fig 6 (Continued)

analysis. (d) A Sankey diagram of multi-omics networks in glioma. The size of each rectangle shows the degree of connectivity of each bacteria, gene, or metabolite. (e) Arthrobacter causally contributed to RFK through N-acetylglutamic-acid ($P_{mediation}$ = 0.02). (f) *Longibaculum* causally contributed to GRIN2B through PC(22:5(7Z,10Z,13Z,16Z,19Z)/22:4(7Z,10Z,13Z,16Z)) ($P_{mediation}$ = 0.016). (g) *Limosilactobacillus* causally contributed to RIMKLA through (R)-*N*-methylsalsolinol ($P_{mediation}$ = 0.042). The gray lines indicate the associations among bacteria, metabolites, and genes, with corresponding $r^{Spearman}$ values and *P*-values. The red arrowed lines indicate the bacterial effects on gene expression mediated by metabolites, with the corresponding mediation *P*-values.

N-acetylglutamic-acid, PC(22:5(7Z,10Z,13Z,16Z,19Z)/22:4(7Z,10Z,13Z,16Z)) and (R)-*N*-methylsalsolinol displayed correlations with some characteristic bacteria and some differentially expressed genes (Fig. 6d). Notably, mediation analysis showed that *Arthrobacter* causally contributed to riboflavin kinase (RFK) through *N*-acetylglutamic-acid ($P_{mediation}$ = 0.02) (Fig. 6e). Additionally, *Longibaculum* causally contributed to glutamate ionotropic receptor NMDA type subunit 2B (GRIN2B) through PC(22:5(7Z,10Z,13Z,16Z,19Z)/22:4(7Z,10Z,13Z,16Z)) ($P_{mediation}$ = 0.016) (Fig. 6f). Moreover, *Limosilactobacillus* causally contributed to ribosomal modification protein rimK like family member A (RIMKLA) through (R)-*N*-methylsalsolinol ($P_{mediation}$ = 0.042) (Fig. 6g). *N*-acetylglutamic-acid (NAG) has been found to be involved in the regulation of NAAG degradation (15). RFK, also known as riboflavin kinase, is the enzyme responsible for synthesizing flavin mononucleotide (FMN) (16). Evidence suggests that FMN can improve the degeneration of dopaminergic neurons (17). PC(22:5(7Z,10Z,13Z,16Z,19Z)/22:4(7Z,10Z,13Z,16Z)) represents a phosphatidylcholine containing docosapentaenoic acid (DPA), which has been detected in the metabolomics of a variety of neurologic diseases (18). DPA is an omega-3 polyunsaturated fatty acid with protective effects on neurons (19). GRIN2B is a subunit of the NMDA receptor, which plays a crucial role in neural development (20), and is implicated for the communication between gut microbiota and the brain (21). RIMKLA, also known as ribosomal modification protein rimK-like family member A, has been identified as the synthetase of NAAG (22). In conclusion, our integrative analysis indicated that intratumoral microbiota of glioma may affect the expression of neuron-related genes through some metabolites related to neuronal function.

Integration of the transcriptome and metabolome analysis reveals the potential role of *Fusobacterium nucleatum* in glioma mouse model

Remarkably, we detected an abundance of *Fusobacterium* in glioma tumor tissue (Fig. 2e). To further confirm the presence of *Fusobacterium* in glioma, we stained human glioma tissue and matched adjacent normal tissue samples using Cy3-labeled *Fusobacterium* probe. As shown by the results, *Fusobacterium* levels in the tumor samples were higher than those in the matched normal brain tissue (see Fig. S8a and b in the supplemental material). Given that *Fusobacterium nucleatum* (Fn) accelerates the development of colorectal (23) and breast (24) cancers, we used the subcutaneous glioma xenograft mouse model to examine whether it also affects tumor progression in glioma, following the scheme in Fig. 7a. Briefly, mice were divided into four groups and performed intratumoral injections of PBS, Fn, metronidazole (MTZ), or Fn combined with MTZ. Figure 7b shows that Fn group had a much larger tumor weight than the PBS and Fn+MTZ groups. Consistently, the trend persisted when evaluating tumor size (Fig. 7c). These results suggest that Fn accelerates tumor growth, while Fn-induced tumor exacerbation can be prevented by metronidazole treatment.

To gain deeper insights into the specific mechanism underlying Fn promotion of glioma growth, we collected tumor tissues from the four mouse groups and performed a transcriptomic analysis. The differentially expressed genes among these groups are detailed in Table S4 in the supplemental material. Venn diagram revealed that there were 70 genes overlapping between Fn vs PBS group and Fn vs Fn + MTZ group, which were not in Fn + MTZ vs MTZ group (see Fig. S9a). Subsequently, we performed KEGG pathway enrichment analysis on these 70 genes, leading to the identification

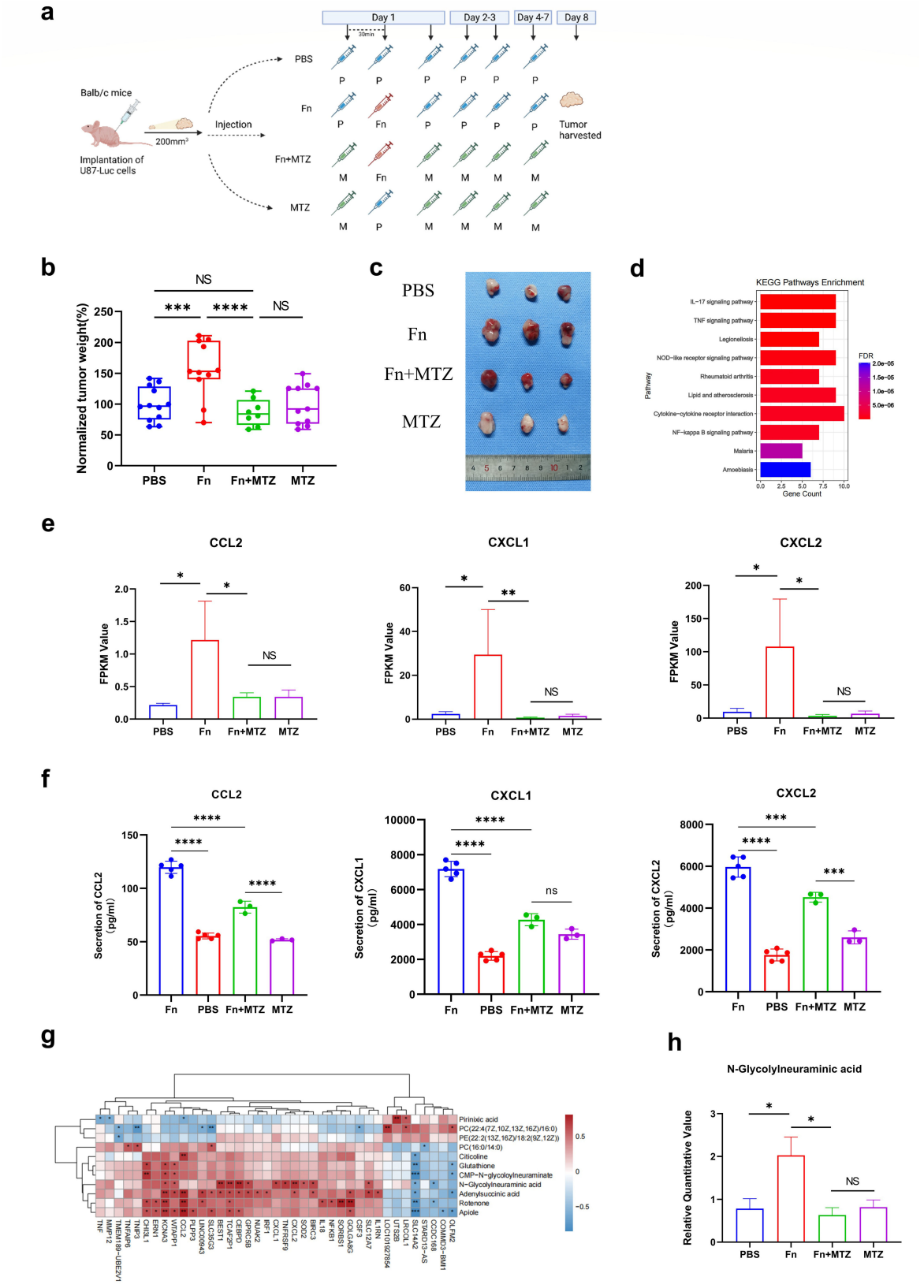

FIG 7 *Fusobacterium nucleatum* accelerates tumor growth in glioma mouse model. (a) Schematic figure of generating subcutaneous glioma xenograft mouse model, the mice receiving intratumoral injections of PBS, Fusobacterium nucleatum (Fn), Fn along with metronidazole (MTZ) treatment or metronidazole, and tumor harvested. (b) Tumor weights were normalized as percentages relative to the average tumor weight in the PBS group for each experiment (set as 100%

(Continued on next page)

Fig 7 (Continued)

tumor weight). Each symbol represents one mouse. (c) Representative tumors post-harvest. (d) The top 10 Bar diagram of KEGG pathway enrichment analysis of differentially expressed genes in tumor tissues from the PBS group, Fn group and Fn + MTZ group. (e) FKPM value of CCL2, CXCL1, and CXCL2 in the PBS, Fn, Fn + MTZ, and MTZ groups following transcriptomics analysis of respective tumor tissues. (f) Protein expression levels of CCL2, CXCL1, and CXCL2 in the PBS (n = 4), Fn (n = 5), Fn + MTZ (n = 3), and MTZ groups (n = 3), measured by ELISA. Statistical method: Student's t-test. (g) Heatmap of Spearman correlation analysis between differential metabolites and some differentially expressed genes with obvious correlation. (h) Relative quantitative value of *N*-glycolylneuraminic acid in the PBS, Fn, Fn + MTZ, and MTZ groups following metabolomic analysis of respective tumor tissues. ****P < 0.0001; ***P < 0.001**P < 0.01; *P < 0.05; NS, not significant. n = 3.

of significant gathering of IL-17 signaling pathway and TNF signaling pathway (Fig. 7d). Since CCL2, CXCL1, and CXCL2 were enriched in both pathways, we performed differential analysis of these three genes. The results revealed that the expression levels of CCL2, CXCL1, and CXCL2 of the Fn group were markedly higher compared to those in the other three groups (Fig. 7e). Notably, previous studies have revealed the close association of these genes with Fn in promoting tumor progression (25–27). In addition, the ELISA assay validated the results of the differential gene expression analysis of CCL2, CXCL1, and CXCL2 in these four groups (Fig. 7f).

Furthermore, we conducted metabolomic analyses on four groups of mouse tumor tissues that received distinct treatments. The differential metabolites among these groups are detailed in Table S5 in the supplemental material. Venn diagram revealed the presence of 11 metabolites that overlapped between Fn vs PBS group and Fn vs Fn + MTZ group but were not observed in Fn + MTZ vs MTZ group (see Fig. S9b). Subsequently, we performed a correlation analysis between these 11 differential metabolites and the 70 differentially expressed genes. Notably, *N*-glycolylneuraminic acid exhibited a strong correlation with numerous differentially expressed genes (Fig. 7f). Furthermore, Fig. 7g visually illustrates that the expression of *N*-glycolylneuraminic acid in the Fn group was remarkably higher compared to those in the other three groups. Remarkably, as a sialic acid, *N*-glycolylneuraminic acid (Neu5Gc) is regarded as a potential human cancer biomarker (28). Previous studies have reported the abundance of Neu5Gc in mouse brain tumor tissues (29). Together, these data suggested that Fn promoted glioma growth by increasing the levels of *N*-acetylneuraminic acid and the expression of CCL2, CXCL1, and CXCL2.

Fusobacterium nucleatum promotes glioma proliferation and upregulates CXCL2 levels in an *in vitro* model

To better simulate clinical conditions, we established patient-derived glioma organoid models to further validate the effect of Fn on promoting glioma proliferation and co-cultured it with Fn (Fig. 8a and b). Then, we measured glioma organoid viability using the ATP assay, following the methods outlined in previous research (30). The results demonstrated that organoids co-cultured with Fn had higher viability than the control group (Fig. 8c). After 2 days of co-culture, we observed that the organoids co-cultured with Fn exhibited larger diameters than the control group (Fig. 8d). After 5 days of co-culture, we collected the organoids, prepared paraffin-embedded sections, and performed Ki67 staining. The results showed higher Ki67 expression in the Fn co-cultured organoids compared to the control group (Fig. 8e). Similarly, we also tested the effect of Fn on glioma cell proliferation in different glioma cell lines. Consistently, glioma cells co-cultured with Fn exhibited higher proliferation rates compared to the control group (see Fig. S10a and b in the supplemental material). These results collectively indicate that Fn treatment promotes glioma proliferation.

DISCUSSION

Since the first identification of intratumoral bacteria in solid tumors, the tumor microbiome has been a focus of cancer research. Currently, 16S rRNA gene sequencing,

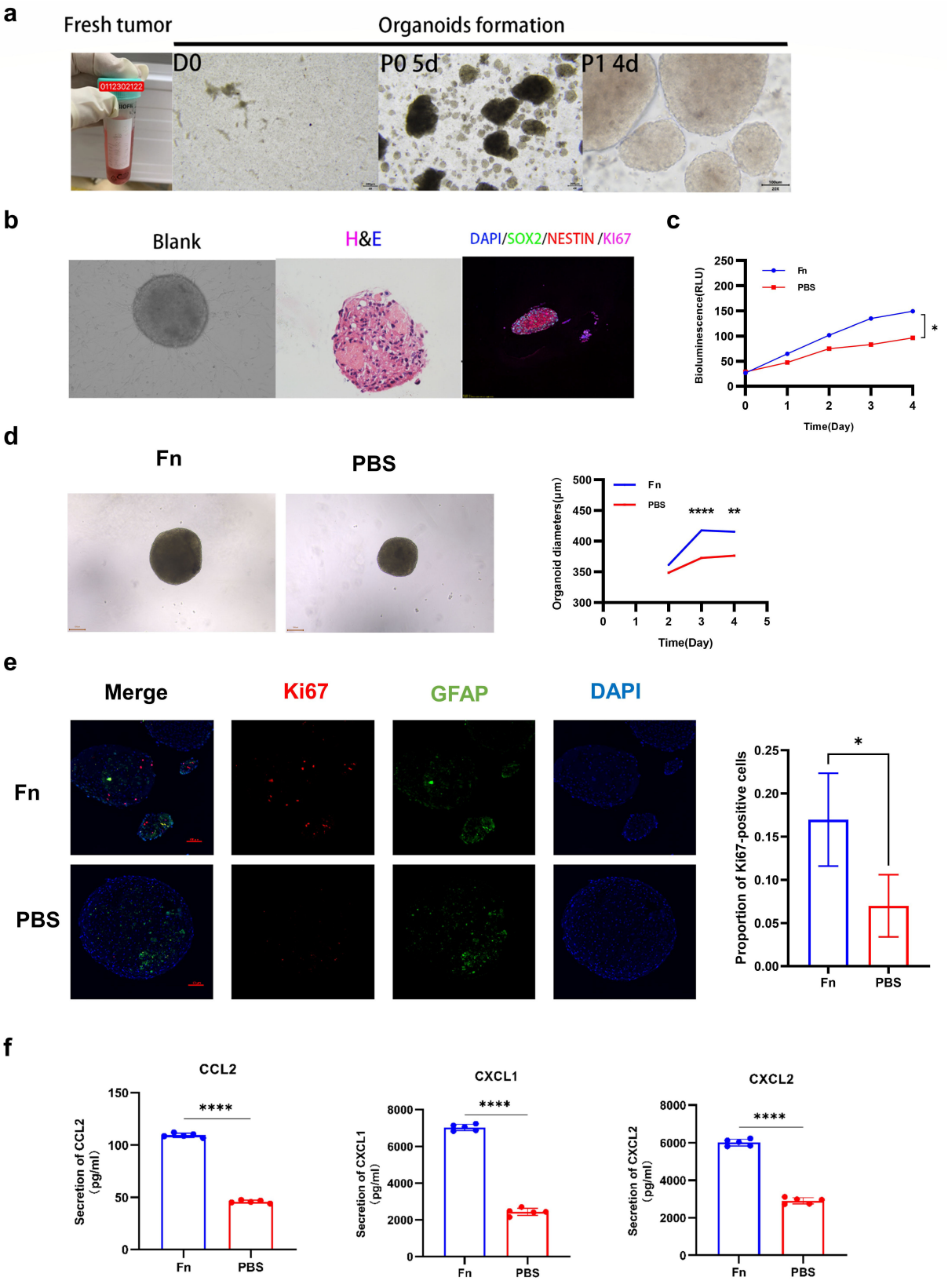

FIG 8 *Fusobacterium nucleatum* improves glioma organoid proliferation. (a) Acquisition of fresh glioma tissue, isolation, and culture of glioma organoids. (b) Growth morphology of untreated glioma organoids (Blank), hematoxylin and eosin (H&E) staining, and immunostaining for neural cell markers. (c) Viability of Fn-organoid and PBS-organoid groups at different time points assessed by ATP assay. Statistical method: one-way ANOVA followed by Bonferroni's multiple

(Continued on next page)

Fig 8 (Continued)

comparison test. (d) Morphological comparison between Fn-organoid and PBS-organoid groups, and diameter measurement of organoids at different time points. Statistical method: one-way ANOVA followed by Bonferroni's multiple comparison test. (e) Immunofluorescence analysis of Ki67 and GFAP protein expression in Fn-organoid and PBS-organoid groups, with a comparison of the proportion of Ki67-positive cells between the two groups. Statistical method: Student's *t*-test. (f) Protein expression levels of CCL2, CXCL1, and CXCL2 in Fn-organoid and PBS-organoid groups measured by ELISA. Statistical method: Student's *t*-test. *($P < 0.05$), **($P < 0.01$), ***($P < 0.001$), Fn (*Fusobacterium nucleatum*).

immunohistochemistry staining, and multi-omics techniques that combine genomics, transcriptomics, proteomics, and metabolomics are powerful analytical methods for characterizing the tumor microbiome (30, 31). In this study, we identified bacteria enriched in glioma tissues by 16S rRNA gene sequencing, verified the presence of bacterial LPS and RNA by morphological experiments, and used multi-omics techniques to explore the interaction between intratumoral microbes and the tumor microenvironment although further experiments are needed to validate these clues. In addition, we also attempted to address the issue of contamination filtering in the tumor microbiome. We mainly followed the contamination filtering method described by Nejman et al. (9) and Fu et al. (3), which involved collecting negative control samples during sample collection and processing, and performing contamination correction in the analysis.

With the growing attention to the gut-brain axis (31), the gut microbiota has been found to be involved in the development, progression, and treatment of glioma by metabolically modulating the epigenetic (32) and immune microenvironments (33). Recently, emerging evidence has also shown a potential function of the intratumoral microbiome in tumor behavior (34) and treatment responses (35). It is of great importance for cancer therapy to elucidate the molecular features of distinct tumor subtypes and predict clinical prognosis from a microbiome perspective. By analyzing 16S rRNA gene sequencing data, we identified six differential bacteria in glioma tissues compared to matched relatively normal brain tissues, including *Fusobacterium*, *Longibaculum*, *Intestinimonas*, *Pasteurella*, *Limosilactobacillus,* and *Arthrobacter*. It is well known that tumor hypoxia, a centerpiece of disease progression mechanisms, is also a common pathological feature in glioma. We found that most of the genera enriched in glioma tissue were anaerobic, which does not seem to be a coincidence. In fact, the high degree of hypoxia in the tumor, immunosuppressive microenvironment, and disturbed vascular system are favorable conditions for rapid bacterial colonization, growth, and replication within the tumor (36).

Furthermore, we observed a marked discrepancy between the microbial composition of fecal samples and tumor samples from the same cohort of glioma patients. This implies that the gut microbiota is not the only possible source of intratumoral bacteria in glioma. These bacteria may also originate from the oral cavity or adjacent brain tissue. We make the following speculations: (i) glioma might change the local microenvironment, such as blood–brain barrier disruption and immunosuppression, which enables bacteria to infiltrate the tumor through the hematogenous or neuronal retrograde pathways. (ii) These bacteria could have been present in the brain tissue prior to tumorigenesis and those that adapted to the tumor microenvironment survive and grow during tumor development. Of course, these speculations should be investigated in future studies.

Fusobacterium is a genus of obligate anaerobic rods, and *Fusobacterium nucleatum* has been reported as a bacterium closely related to tumorigenesis (37). *Fusobacterium* was found to be enriched in stool samples from glioma patients (38). Here, it was found to be enriched in the tumor tissues of glioma patients. *Longibaculum*, belonging to the bacterial genus within the family *Erysipelotrichaceae*, has not been extensively investigated in the context of glioma. However, studies have indicated its involvement in weight-independent improvement of blood glucose subsequent to gastric bypass surgery (39). In a mouse model of glioma, *Intestinimonas* was reported to exhibit a continuous increase in abundance during the progression of tumor growth in a mouse model of glioma (40). Remarkably, *Intestinimonas* possesses distinctive metabolic

capabilities that allow it to produce butyrate from both carbohydrates and amino acids (41). *Pasteurella* is a genus of opportunistic pathogens, and one of its species, *Pasteurella multocida*, has been reported to cause bacterial meningitis (42). Although investigations thus far have not illuminated any direct link between *Pasteurella* and glioma, the presence of *Pasteurella multocida* toxin (PMT), characterized by profound mitogenic activity and carcinogenic potential (43), presents an intriguing possibility. It is conceivable that PMT may serve as a pivotal mediator of the association between *Pasteurella* and glioma pathogenesis. *Limosilactobacillus reuteri*, extensively studied for its protective properties (44), has recently been implicated in the induction of multiple sclerosis (45). *Arthrobacter* strain NOR5 has exhibited remarkable proficiency in facilitating the complete degradation of nornicotine (46), a direct precursor of tobacco-specific nitrosamines (TSNAs) known for their potent carcinogenic properties (47). Furthermore, *Arthrobacter citreus* strains can metabolize caprolactam, thereby generating glutamate (48)-an important excitatory neurotransmitter in the central nervous system. Based on these findings, it becomes conceivable that Arthrobacter holds probiotic potential. Notably, our investigation also revealed an association between Arthrobacter and NAA as well as NAAG.

It is undeniable that culturing bacteria from fresh glioma tissues is the critical evidence for their presence. Regrettably, our endeavors in bacterial culture encountered setbacks. Our efforts resulted solely in the cultivation of *Pseudomonas stutzeri*, a bacterium that has exhibited resistance against multiple antibiotics (data not shown). We speculate that this outcome may be attributed to the constraints posed by current medical practices, particularly the widespread utilization of prophylactic antibiotics.

Furthermore, a noteworthy observation in our study was the notable elevation of LPS signals in glioma tissue in stark contrast to adjacent normal brain tissue. LPS, a prevalent endotoxin, displays the capacity to interact with Toll-like receptor 4 (TLR4) *in vivo*, provoking the activation of monocytes and macrophages, thereby instigating the synthesizing and subsequent release of various cytokines and inflammatory mediators (49). Remarkably, investigations have illustrated that glioblastoma clinical samples exhibit heightened expression levels of TLR4 (50), corroborating the findings of our study. Moreover, we also found that LPS signals were more prevalent in tumor cell-enriched regions, while macrophage-enriched regions had fewer signals. We propose that this may result from LPS-induced macrophage activation and subsequent phagocytic clearance by macrophages. Notably, alongside bacterial LPS, RNA, and DNA found in human gliomas, recent studies have unraveled the presence of bacterial-derived peptides on human leukocyte antigen molecules in glioblastoma (51). These peptides elicit strong responses from tumor-infiltrating lymphocytes and peripheral blood memory cells, suggesting that microbial peptides activate tumor-infiltrating lymphocytes in glioblastoma.

In addition, we performed transcriptomic sequencing on glioma tissues derived from patients simultaneously. We found that 28 differentially expressed genes associated with six different bacterial genera were enriched in pathways such as serotonergic synapse, cholinergic synapse, glutamatergic synapse, and dopaminergic synapse. The integrated omics analysis revealed that intratumoral microbiome may affect the expression of neuron-related genes through bacteria-associated metabolites. Previous review articles have highlighted the ability of gliomas to exploit normal mechanisms of neuronal development and plasticity, leading to the formation of neuron-glia synapses with subsequent enhancement of glioma proliferation (52). Building upon these limited but intriguing pieces of evidence, we speculate that the intratumoral bacteria in glioma may be involved in the formation of neuron-glia synapses.

Additionally, a noteworthy discovery emerged as we unraveled the association of HTR1D and STAT4 with the characteristic bacteria and the majority of the differential metabolites. HTR1D, a type of 5-hydroxytryptamine (5-HT) receptor, activates intracellular signaling pathways through G proteins upon binding to serotonin (53). Such signal transduction represents a fundamental process mediated by the monoamine

neurotransmitter 5-HT. Consequently, HTR1D may be an important molecule in the neuron-glia synapses involved by intratumoral bacteria of glioma. Concurrently, STAT4 operates as a transcription factor. Prior studies employing the Oncomine database scrutinized the mRNA expression levels of STAT gene family members in glioma, revealing diminished STAT4 mRNA expression in comparison to that observed in normal controls (54)—an observation corroborated by our own inquiry. Of equal import, several studies have unveiled STAT4's pivotal role in regulating neutrophil function, as demonstrated by the impact of STAT4 deficiency on neutrophil extracellular trap formation and antibacterial immunity (55). Therefore, within the context of intratumoral bacteria-associated glioma, STAT4 emerges as an indispensable molecule in tumor-associated immune regulation.

We found Fn promotes glioma proliferation and upregulates CCL2, CXCL1, and CXCL2 levels *in vivo* and *in vitro* models of glioma. A recent study found that Fn induces the secretion of pro-inflammatory cytokines, including CCL2 and CXCL1, through bacterial surface adhesin Fap2 (25), DNA hunger/stationary phase protective proteins (Dps) (56), or CXCL2-mediated crosstalk between tumor cells and macrophages (57). Besides, intratumoral F. nucleatum promotes pancreatic cancer progression through autocrine and paracrine mechanisms of the CXCL1-CXCR2 axis (58). Additionally, in the glioma microenvironment, upregulation of CCL2 promotes the infiltration of tumor-associated macrophages, which, in turn, promotes the proliferation and survival of glioblastoma cells by transferring LDHA-containing extracellular vesicles (59). Elevated levels of CXCL1 or CXCL2 promote myeloid cell migration while disrupting the accumulation of CD8 T cells at the tumor site, leading to accelerated glioblastoma progression. These findings provide us with potential mechanisms. We will further explore the specific mechanisms by which Fn upregulates cytokines such as CCL2, CXCL1, and CXCL2 to promote glioma development in future studies.

The relationship between intratumoral bacteria and host cells in the tumor microenvironment is a key area of interest. In this study, we conducted a preliminary investigation into the distribution of bacterial LPS signals in tumor cells and macrophages, but LPS and CD68 are not specific markers for bacteria and macrophages. Flow cytometry could provide more accurate quantitative information on bacteria within macrophages and tumor cells to some extent. Proteomics and single-cell RNA sequencing are necessary to further understand the interactions between microbes and the host. In addition, for a more comprehensive understanding, new techniques like spatial metatranscriptomics (60) and InvadeSeq (invasion-adhesion-directed expression sequencing) (61) can be considered. These methods can simultaneously capture both bacterial and host RNA information from tissue sections, providing *in situ* insights into functional interactions between microbes and host cells in the tumor microenvironment. Furthermore, given that microbes often interact with the host through metabolites, we could also consider using the metaFISH method (62). This technique combines the high resolution of fluorescence microscopy, the specificity of FISH probes, and high-resolution MALDI-MSI to map the spatial distribution of metabolites at the cellular level. This could help us better understand the communication, defense, and nutrient exchange between host and microbes. These advanced technologies offer new perspectives for investigating microbial-host interactions in future studies.

Previous studies have demonstrated the ability of *Fusobacterium nucleatum* to confer resistance to chemotherapy (63) and the enhancement of PD-L1 blockers (64) in colorectal cancer. Given the enrichment of Fn observed in glioma and its capability to induce the production of chemokines, it becomes crucial to explore the potential associations between Fn and temozolomide, a first-line chemotherapy drug for glioma, as well as the interplay between Fn and PD-L1 in glioma context. These avenues of investigation hold considerable promise for future research endeavors. The advancement of bacterial engineering technology is an exciting opportunity to develop specifically modified bacteria that can serve as anti-tumor carriers. We have previously explored the potential mechanism of genetically engineered bacteria Salmonella YB1

in the treatment of glioma and found that Salmonella YB1 inhibits the expression of glutathione peroxidase-4 and induces ferroptosis to suppress glioma growth (59). The key bacteria identified in this study may be considered potential engineered bacteria for glioma treatment.

Despite the significance of our findings, our study has certain limitations. First, the postulated interactions between the intratumoral bacteria and glioma necessitate validation through targeted experiment investigations. Second, our study sample size was relatively small, highlighting the need for multicenter, large sample studies to elucidate the relationship between key bacteria, their related metabolites, and glioma prognosis. Third, even though we referred to the existing and well-recognized methods for identifying intratumoral microbiota, we still could not completely eliminate the internal contamination from samples and the external contamination from the environment. Therefore, the analytical methods for contamination filtering in the tumor microbiome should be improved and standardized in the future.

Nevertheless, our study provides insights into the intricate interplay between intratumoral bacteria and glioma, potentially inspiring new avenues of exploration in glioma biology. Looking ahead, an in-depth study of the intratumoral microbiota holds immense promise for advancing anti-cancer treatment.

Conclusion

Overall, a multi-omics analysis of human glioma tissue showed that the intratumoral microbiome may affect the expression of neuron-related genes through bacteria-associated metabolites. Both *in vivo* and *in vitro* experiments demonstrated that Fn, as a key bacterium enriched in glioma tissue, promotes glioma proliferation and increases the expression of CCL2, CXCL1, and CXCL2. Our work reveals the oncogenic roles of Fn and suggests that Fn could be a potential diagnostic and therapeutic target for glioma patients.

ACKNOWLEDGMENTS

Thanks go to Dr. SongHe Guo for the kind gift of the strain ATCC25586 (*Fusobacterium nucleatum*) and assistance with bacterial culture. Thanks go to Dr. Zhang Xin for her assistance and guidance in the cultivation of glioma organoids. Thanks go to Dr. Yan He and Dr. Jiayuan Huang for carefully reading the article and giving valuable suggestions. We also thank all staff at the technical staff of the Clinical Biobank Centre for their kind assistance. Finally, we thank all tissue donors and their families who have kindly donated their resected specimens to the Clinical Biobank Centre. We acknowledge Biorender, since figures were made using this software.

The research was supported by Guangdong Basic and Applied Basic Research Foundation (2023A1515030045) and the Presidential Foundation of Zhujiang Hospital of Southern Medical University (yzjj2022ms4).

H.S. conceptualized the project, designed and supervised the study. T.L. and Z.Z. performed experiments and drafted the manuscript. M.P., L.Z., and C.W. participated in the execution of experiments and data analysis. F.L. polished the English language. M.Z., K.S., and Z.F. participated in the data analysis. C.L. directed the culture of organoid. Y.L. and Y.X. participated in the collection of samples. J.W. participated in analysis and interpretation of data. J.-D.H. and H.Z. participated in the study supervision. All authors contributed to writing the manuscript, provided critical feedback during editing, and approved the final submitted version.

AUTHOR AFFILIATIONS

[1]Clinical Biobank Center, Microbiome Medicine Center, Department of Laboratory Medicine, Guangdong Provincial Clinical Research Center for Laboratory Medicine, Zhujiang Hospital, Southern Medical University, Guangzhou, China

[2]Neurosurgery Center, The National Key Clinical Specialty, The Engineering Technology Research Center of Education Ministry of China on Diagnosis and Treatment of Cerebrovascular Disease, Guangdong Provincial Key Laboratory on Brain Function Repair and Regeneration, The Neurosurgery Institute of Guangdong Province Zhujiang Hospital, Southern Medical University, Guangzhou, China
[3]School of Biomedical Sciences, Li Ka Shing Faculty of Medicine, University of Hong Kong, Hong Kong Special Administrative Region, China
[4]Chinese Academy of Sciences (CAS) Key Laboratory of Quantitative Engineering Biology, Shenzhen Institute of Synthetic Biology, Shenzhen Institutes of Advanced Technology, Chinese Academy of Sciences, Shenzhen, China
[5]Clinical Oncology Center, Shenzhen Key Laboratory for Cancer Metastasis and Personalized Therapy, The University of Hong Kong-Shenzhen Hospital, Shenzhen, China
[6]Guangdong-Hong Kong Joint Laboratory for RNA Medicine, Sun Yat-Sen University, Guangzhou, China
[7]Key Laboratory of Mental Health of the Ministry of Education, Guangdong-Hong Kong-Macao Greater Bay Area Center for Brain Science and Brain-Inspired Intelligence, Southern Medical University, Guangzhou, China

AUTHOR ORCIDs

Ting Li http://orcid.org/0000-0002-2335-4886
Haitao Sun http://orcid.org/0000-0001-7925-9506

FUNDING

Funder	Grant(s)	Author(s)
Guangdong basic and applied basic research foundation	2023A1515030045	Haitao Sun
Presidential Foundation of Zhujiang Hospital of Sounthern Medical University	yzjj2022ms4	Haitao Sun

DATA AVAILABILITY

The raw sequence data reported in this paper have been deposited in the Genome Sequence Archive (65, 66) in National Genomics Data Center, China National Center for Bioinformation/Beijing Institute of Genomics, Chinese Academy of Sciences (GSA-Human: HRA005548 and HRA005686). The metabolomics data reported in this paper have been deposited in the OMIX under the accession no. OMIX004935 and OMIX004936. All other data supporting the findings of this study are available within the article, in the supplemental material, or from the corresponding authors upon reasonable request. A STORMS (Strengthening The Organizing and Reporting of Microbiome Studies) checklist (67) is available at the following DOI: 10.5281/zenodo.13981309.

ETHICS APPROVAL

The study received the informed consent of patients and was approved by the local Ethics Committee (2018-SJWK-004) (2022-KY-KY-102-02). The registration has been completed on the website of the China Clinical Trial Registry Center (ChiCTR2300067789). The Animal Ethics Committee of Southern Medical University approved the animal study, which was performed according to National Institutes of Health guidelines (Approval ID: LAEC-2022-197).

ADDITIONAL FILES

The following material is available online.

Supplemental Material

Supplemental Figures (mSystems00457-24-s0001.pdf). Figures S1 to S10.

Supplemental Methods (mSystems00457-24-s0002.pdf). Additional details for multiplex immunofluorescent assay, 16S rRNA FISH, DNA extraction and sequencing, mRNA-seq, and metabolomics.
Table S1 (mSystems00457-24-s0003.xlsx). Clinical data of glioma patients.
Table S2 (mSystems00457-24-s0004.xlsx). Differentially expressed genes in human glioma tissues.
Table S3 (mSystems00457-24-s0005.xlsx). Differential metabolites in human glioma tissues.
Table S4 (mSystems00457-24-s0006.xlsx). Differentially expressed genes in mouse tumor tissues.
Table S5 (mSystems00457-24-s0007.xlsx). Differential metabolites in mouse tumor tissues.

REFERENCES

1. Sung H, Ferlay J, Siegel RL, Laversanne M, Soerjomataram I, Jemal A, Bray F. 2021. Global cancer statistics 2020: GLOBOCAN estimates of incidence and mortality worldwide for 36 cancers in 185 countries. CA Cancer J Clin 71:209–249. https://doi.org/10.3322/caac.21660
2. Jin C, Lagoudas GK, Zhao C, Bullman S, Bhutkar A, Hu B, Ameh S, Sandel D, Liang XS, Mazzilli S, Whary MT, Meyerson M, Germain R, Blainey PC, Fox JG, Jacks T. 2019. Commensal microbiota promote lung cancer development via γδ T cells. Cell 176:998–1013. https://doi.org/10.1016/j.cell.2018.12.040
3. Fu A, Yao B, Dong T, Chen Y, Yao J, Liu Y, Li H, Bai H, Liu X, Zhang Y, Wang C, Guo Y, Li N, Cai S. 2022. Tumor-resident intracellular microbiota promotes metastatic colonization in breast cancer. Cell 185:1356–1372. https://doi.org/10.1016/j.cell.2022.02.027
4. Qiao H, Tan X-R, Li H, Li J-Y, Chen X-Z, Li Y-Q, Li W-F, Tang L-L, Zhou G-Q, Zhang Y, Liang Y-L, He Q-M, Zhao Y, Huang S-Y, Gong S, Li Q, Ye M-L, Chen K-L, Sun Y, Ma J, Liu N. 2022. Association of intratumoral microbiota with prognosis in patients with nasopharyngeal carcinoma from 2 hospitals in China. JAMA Oncol 8:1301–1309. https://doi.org/10.1001/jamaoncol.2022.2810
5. Wang Q, Yang Q, Liu X. 2023. The microbiota-gut-brain axis and neurodevelopmental disorders. Protein Cell 14:762–775. https://doi.org/10.1093/procel/pwad026
6. Dominy SS, Lynch C, Ermini F, Benedyk M, Marczyk A, Konradi A, Nguyen M, Haditsch U, Raha D, Griffin C, et al. 2019. *Porphyromonas gingivalis* in Alzheimer's disease brains: evidence for disease causation and treatment with small-molecule inhibitors. Sci Adv 5:eaau3333. https://doi.org/10.1126/sciadv.aau3333
7. Zhan X, Stamova B, Jin L-W, DeCarli C, Phinney B, Sharp FR. 2016. Gram-negative bacterial molecules associate with Alzheimer disease pathology. Neurol (ECronicon) 87:2324–2332. https://doi.org/10.1212/WNL.0000000000003391
8. Zhao Y, Jaber V, Lukiw WJ. 2017. Secretory products of the human GI tract microbiome and their potential impact on Alzheimer's disease (AD): detection of lipopolysaccharide (LPS) in AD hippocampus. Front Cell Infect Microbiol 7:318. https://doi.org/10.3389/fcimb.2017.00318
9. Nejman D, Livyatan I, Fuks G, Gavert N, Zwang Y, Geller LT, Rotter-Maskowitz A, Weiser R, Mallel G, Gigi E, et al. 2020. The human tumor microbiome is composed of tumor type-specific intracellular bacteria. Science 368:973–980. https://doi.org/10.1126/science.aay9189
10. Zhao J, He D, Lai HM, Xu Y, Luo Y, Li T, Liang J, Yang X, Guo L, Ke Y, Zhou H, Wu W, Guo H, Sun H. 2022. Comprehensive histological imaging of native microbiota in human glioma. J Biophotonics 15:e202100351. https://doi.org/10.1002/jbio.202100351
11. Westfall S, Dinh DM, Pasinetti GM. 2020. Investigation of potential brain microbiome in Alzheimer's disease: implications of study bias. J Alzheimers Dis 75:559–570. https://doi.org/10.3233/JAD-191328
12. Maruyama W, Narabayashi H, Dostert P, Naoi M. 1996. Stereospecific occurrence of a Parkinsonism-inducing catechol isoquinoline, n-methyl(R)salsolinol, in the human intraventricular fluid. J Neural Transm (Vienna) 103:1069–1076. https://doi.org/10.1007/BF01291791
13. Long PM, Moffett JR, Namboodiri AMA, Viapiano MS, Lawler SE, Jaworski DM. 2013. *N*-acetylaspartate (NAA) and *N*-acetylaspartylglutamate (NAAG) promote growth and inhibit differentiation of glioma stem-like cells. J Biol Chem 288:26188–26200. https://doi.org/10.1074/jbc.M113.487553
14. Lee CJ, Qiu TA, Sweedler JV. 2020. D-alanine: distribution, origin, physiological relevance, and implications in disease. Biochim Biophys Acta Proteins Proteom 1868:140482. https://doi.org/10.1016/j.bbapap.2020.140482
15. Alonso E, García-Pérez MA, Bueso J, Rubio V. 1991. N-acetyl-L-glutamate in brain: assay, levels, and regional and subcellular distribution. Neurochem Res 16:787–794. https://doi.org/10.1007/BF00965688
16. Hirano G, Izumi H, Yasuniwa Y, Shimajiri S, Ke-Yong W, Sasagiri Y, Kusaba H, Matsumoto K, Hasegawa T, Akimoto M, Akashi K, Kohno K. 2011. Involvement of riboflavin kinase expression in cellular sensitivity against cisplatin. Int J Oncol 38:893–902. https://doi.org/10.3892/ijo.2011.938
17. Gong J, Zhang W, Ding L, Zhang M, Zheng S, Ma R, Tang J, Yi W, Xu H, Zhang Y. 2021. 4,4'-Dimethoxychalcone regulates redox homeostasis by targeting riboflavin metabolism in Parkinson's disease therapy. Free Radic Biol Med 174:40–56. https://doi.org/10.1016/j.freeradbiomed.2021.07.038
18. Cao C, Li Q, Chen Y, Zou M, Sun C, Li X, Wu L. 2023. Untargeted metabolomic analysis reveals the metabolic disturbances and exacerbation of oxidative stress in the cerebral cortex of a BTBR mouse model of autism. J Mol Neurosci 73:15–27. https://doi.org/10.1007/s12031-022-02096-6
19. Liu B, Zhang Y, Yang Z, Liu M, Zhang C, Zhao Y, Song C. 2021. ω-3 DPA protected neurons from neuroinflammation by balancing microglia M1/M2 polarizations through inhibiting NF-κB/MAPK p38 signaling and activating neuron-BDNF-PI3K/AKT pathways. Mar Drugs 19:11. https://doi.org/10.3390/md19110587
20. Sabo SL, Lahr JM, Offer M, Weekes AL, Sceniak MP. 2022. *GRIN2B*-related neurodevelopmental disorder: current understanding of pathophysiological mechanisms. Front Synaptic Neurosci 14:1090865. https://doi.org/10.3389/fnsyn.2022.1090865
21. Fröhlich EE, Farzi A, Mayerhofer R, Reichmann F, Jačan A, Wagner B, Zinser E, Bordag N, Magnes C, Fröhlich E, Kashofer K, Gorkiewicz G, Holzer P. 2016. Cognitive impairment by antibiotic-induced gut dysbiosis: analysis of gut microbiota-brain communication. Brain Behav Immun 56:140–155. https://doi.org/10.1016/j.bbi.2016.02.020
22. Lodder-Gadaczek J, Becker I, Gieselmann V, Wang-Eckhardt L, Eckhardt M. 2011. *N*-acetylaspartylglutamate synthetase II synthesizes *N*-acetylaspartylglutamylglutamate. J Biol Chem 286:16693–16706. https://doi.org/10.1074/jbc.M111.230136
23. Rubinstein MR, Wang X, Liu W, Hao Y, Cai G, Han YW. 2013. *Fusobacterium nucleatum* promotes colorectal carcinogenesis by modulating E-cadherin/β-catenin signaling via its FadA adhesin. Cell Host Microbe 14:195–206. https://doi.org/10.1016/j.chom.2013.07.012
24. Parhi L, Alon-Maimon T, Sol A, Nejman D, Shhadeh A, Fainsod-Levi T, Yajuk O, Isaacson B, Abed J, Maalouf N, Nissan A, Sandbank J, Yehuda-Shnaidman E, Ponath F, Vogel J, Mandelboim O, Granot Z, Straussman R, Bachrach G. 2020. Breast cancer colonization by *Fusobacterium nucleatum* accelerates tumor growth and metastatic progression. Nat Commun 11:3259. https://doi.org/10.1038/s41467-020-16967-2
25. Casasanta MA, Yoo CC, Udayasuryan B, Sanders BE, Umaña A, Zhang Y, Peng H, Duncan AJ, Wang Y, Li L, Verbridge SS, Slade DJ. 2020.

Fusobacterium nucleatum host-cell binding and invasion induces IL-8 and CXCL1 secretion that drives colorectal cancer cell migration. Sci Signal 13:641. https://doi.org/10.1126/scisignal.aba9157
26. Jin X, Kim S-H, Jeon H-M, Beck S, Sohn Y-W, Yin J, Kim J-K, Lim YC, Lee J-H, Kim S-H, Kang S-H, Pian X, Song M-S, Park JB, Chae Y-S, Chung Y-G, Lee S-H, Choi Y-J, Nam D-H, Choi YK, Kim H. 2012. Interferon regulatory factor 7 regulates glioma stem cells via interleukin-6 and Notch signalling. Brain (Bacau) 135:1055–1069. https://doi.org/10.1093/brain/aws028
27. Zhang Q, Wang J, Yao X, Wu S, Tian W, Gan C, Wan X, You C, Hu F, Zhang S, Zhang H, Zhao K, Shu K, Lei T. 2021. Programmed cell death 10 mediated CXCL2-CXCR2 signaling in regulating tumor-associated microglia/macrophages recruitment in glioblastoma. Front Immunol 12:637053. https://doi.org/10.3389/fimmu.2021.637053
28. Wang J, Shewell LK, Day CJ, Jennings MP. 2023. *N*-glycolylneuraminic acid as a carbohydrate cancer biomarker. Transl Oncol 31:101643. https://doi.org/10.1016/j.tranon.2023.101643
29. Seyfried TN, el-Abbadi M, Roy ML. 1992. Ganglioside distribution in murine neural tumors. Mol Chem Neuropathol 17:147–167. https://doi.org/10.1007/BF03159989
30. Driehuis E, Kretzschmar K, Clevers H. 2020. Establishment of patient-derived cancer organoids for drug-screening applications. Nat Protoc 15:3380–3409. https://doi.org/10.1038/s41596-020-0379-4
31. Deidda G, Biazzo M. 2021. Gut and brain: investigating physiological and pathological interactions between microbiota and brain to gain new therapeutic avenues for brain diseases. Front Neurosci 15:753915. https://doi.org/10.3389/fnins.2021.753915
32. Fan Y, Su Q, Chen J, Wang Y, He S. 2022. Gut microbiome alterations affect glioma development and Foxp3 expression in tumor microenvironment in mice. Front Oncol 12:836953. https://doi.org/10.3389/fonc.2022.836953
33. Lyu Y, Yang H, Chen L. 2022. Metabolic regulation on the immune environment of glioma through gut microbiota. Semin Cancer Biol 86:990–997. https://doi.org/10.1016/j.semcancer.2021.05.005
34. Wong-Rolle A, Wei HK, Zhao C, Jin C. 2021. Unexpected guests in the tumor microenvironment: microbiome in cancer. Protein Cell 12:426–435. https://doi.org/10.1007/s13238-020-00813-8
35. Riquelme E, Zhang Y, Zhang L, Montiel M, Zoltan M, Dong W, Quesada P, Sahin I, Chandra V, San Lucas A, et al. 2019. Tumor microbiome diversity and composition influence pancreatic cancer outcomes. Cell 178:795–806. https://doi.org/10.1016/j.cell.2019.07.008
36. Jiang Z, Zhang W, Zhang Z, Sha G, Wang D, Tang D. 2023. Intratumoral microbiota: a new force in diagnosing and treating pancreatic cancer. Cancer Lett 554:216031. https://doi.org/10.1016/j.canlet.2022.216031
37. Kostic AD, Chun E, Robertson L, Glickman JN, Gallini CA, Michaud M, Clancy TE, Chung DC, Lochhead P, Hold GL, El-Omar EM, Brenner D, Fuchs CS, Meyerson M, Garrett WS. 2013. *Fusobacterium nucleatum* potentiates intestinal tumorigenesis and modulates the tumor-immune microenvironment. Cell Host Microbe 14:207–215. https://doi.org/10.1016/j.chom.2013.07.007
38. Jiang H, Zeng W, Zhang X, Pei Y, Zhang H, Li Y. 2022. The role of gut microbiota in patients with benign and malignant brain tumors: a pilot study. Bioengineered 13:7847–7859. https://doi.org/10.1080/21655979.2022.2049959
39. Hankir MK, Kovatcheva-Datchary P, Springer R, Hoffmann A, Vogel J, Seyfried F, Arora T. 2023. Gut microbiota contribution to weight-independent glycemic improvements after gastric bypass surgery. Microbiol Spectr 11:e0510922. https://doi.org/10.1128/spectrum.05109-22
40. Li X-C, Wu B-S, Jiang Y, Li J, Wang Z-F, Ma C, Li Y-R, Yao J, Jin X-Q, Li Z-Q. 2021. Temozolomide-induced changes in gut microbial composition in a mouse model of brain glioma. Drug Des Devel Ther 15:1641–1652. https://doi.org/10.2147/DDDT.S298261
41. Bui TPN, Shetty SA, Lagkouvardos I, Ritari J, Chamlagain B, Douillard FP, Paulin L, Piironen V, Clavel T, Plugge CM, de Vos WM. 2016. Comparative genomics and physiology of the butyrate-producing bacterium Intestinimonas butyriciproducens. Environ Microbiol Rep 8:1024–1037. https://doi.org/10.1111/1758-2229.12483
42. Peng Z, Wang X, Zhou R, Chen H, Wilson BA, Wu B. 2019. *Pasteurella multocida*: genotypes and genomics. Microbiol Mol Biol Rev 83:e00014-19. https://doi.org/10.1128/MMBR.00014-19
43. Preuss I, Hildebrand D, Orth JHC, Aktories K, Kubatzky KF. 2010. *Pasteurella multocida* toxin is a potent activator of anti-apoptotic signalling pathways. Cell Microbiol 12:1174–1185. https://doi.org/10.1111/j.1462-5822.2010.01462.x
44. Mu Q, Tavella VJ, Luo XM. 2018. Role of *Lactobacillus reuteri* in human health and diseases. Front Microbiol 9:757. https://doi.org/10.3389/fmicb.2018.00757
45. Miyauchi E, Kim S-W, Suda W, Kawasumi M, Onawa S, Taguchi-Atarashi N, Morita H, Taylor TD, Hattori M, Ohno H. 2020. Gut microorganisms act together to exacerbate inflammation in spinal cords. Nature 585:102–106. https://doi.org/10.1038/s41586-020-2634-9
46. Najme R, Zhuang S, Qiu J, Lu Z. 2021. Identification and characterization of nornicotine degrading strain *Arthrobacter* sp. NOR5. Sci Total Environ 764:142894. https://doi.org/10.1016/j.scitotenv.2020.142894
47. Chen B, Qian Y, Wu M, Zhu L, Hu B, Li XF. 2015. Identification of precursors and mechanisms of tobacco-specific nitrosamine formation in water during chloramination. Environ Sci Technol 49:459–466. https://doi.org/10.1021/es505057h
48. Baxi NN, Patel S, Hansoti D. 2019. An *Arthrobacter citreus* strain suitable for degrading ε-caprolactam in polyamide waste and accumulation of glutamic acid. AMB Express 9:161. https://doi.org/10.1186/s13568-019-0887-1
49. Ciesielska A, Matyjek M, Kwiatkowska K. 2021. TLR4 and CD14 trafficking and its influence on LPS-induced pro-inflammatory signaling. Cell Mol Life Sci 78:1233–1261. https://doi.org/10.1007/s00018-020-03656-y
50. Han S, Wang C, Qin X, Xia J, Wu A. 2017. LPS alters the immunophenotype of glioma and glioma stem-like cells and induces *in vivo* antitumor immunity via TLR4. J Exp Clin Cancer Res 36:83. https://doi.org/10.1186/s13046-017-0552-y
51. Naghavian R, Faigle W, Oldrati P, Wang J, Toussaint NC, Qiu Y, Medici G, Wacker M, Freudenmann LK, Bonté P-E, Weller M, Regli L, Amigorena S, Rammensee H-G, Walz JS, Brugger SD, Mohme M, Zhao Y, Sospedra M, Neidert MC, Martin R. 2023. Microbial peptides activate tumour-infiltrating lymphocytes in glioblastoma. Nature 617:807–817. https://doi.org/10.1038/s41586-023-06081-w
52. Lim-Fat MJ, Wen PY. 2020. Glioma progression through synaptic activity. Nat Rev Neurol 16:6–7. https://doi.org/10.1038/s41582-019-0290-1
53. Millan MJ, Marin P, Bockaert J, Mannoury la Cour C. 2008. Signaling at G-protein-coupled serotonin receptors: recent advances and future research directions. Trends Pharmacol Sci 29:454–464. https://doi.org/10.1016/j.tips.2008.06.007
54. Ji W, Liu Y, Xu B, Mei J, Cheng C, Xiao Y, Yang K, Huang W, Jiao J, Liu H, Shao J. 2021. Bioinformatics analysis of expression profiles and prognostic values of the signal transducer and activator of transcription family genes in glioma. Front Genet 12:625234. https://doi.org/10.3389/fgene.2021.625234
55. Mehrpouya-Bahrami P, Moriarty AK, De Melo P, Keeter WC, Alakhras NS, Nelson AS, Hoover M, Barrios MS, Nadler JL, Serezani CH, Kaplan MH, Galkina EV. 2021. STAT4 is expressed in neutrophils and promotes antimicrobial immunity. JCI Insight 6:14. https://doi.org/10.1172/jci.insight.141326
56. Wu Y, Guo S, Chen F, Li Y, Huang Y, Liu W, Zhang G. 2023. Fn-Dps, a novel virulence factor of *Fusobacterium nucleatum*, disrupts erythrocytes and promotes metastasis in colorectal cancer. PLoS Pathog 19:e1011096. https://doi.org/10.1371/journal.ppat.1011096
57. Nie F, Zhang J, Tian H, Zhao J, Gong P, Wang H, Wang S, Yang P, Yang C. 2024. The role of CXCL2-mediated crosstalk between tumor cells and macrophages in *Fusobacterium nucleatum*-promoted oral squamous cell carcinoma progression. Cell Death Dis 15:277. https://doi.org/10.1038/s41419-024-06640-7
58. Hayashi M, Ikenaga N, Nakata K, Luo H, Zhong P, Date S, Oyama K, Higashijima N, Kubo A, Iwamoto C, Torata N, Abe T, Yamada Y, Ohuchida K, Oda Y, Nakamura M. 2023. Intratumor *Fusobacterium nucleatum* promotes the progression of pancreatic cancer via the CXCL1-CXCR2 axis. Cancer Sci 114:3666–3678. https://doi.org/10.1111/cas.15901
59. Khan F, Lin Y, Ali H, Pang L, Dunterman M, Hsu W-H, Frenis K, Grant Rowe R, Wainwright DA, McCortney K, Billingham LK, Miska J, Horbinski C, Lesniak MS, Chen P. 2024. Lactate dehydrogenase A regulates tumor-macrophage symbiosis to promote glioblastoma progression. Nat Commun 15:1987. https://doi.org/10.1038/s41467-024-46193-z

60. Saarenpää S, Shalev O, Ashkenazy H, Carlos V, Lundberg DS, Weigel D, Giacomello S. 2024. Spatial metatranscriptomics resolves host-bacteria-fungi interactomes. Nat Biotechnol 42:1384–1393. https://doi.org/10.1038/s41587-023-01979-2
61. Galeano Niño JL, Wu H, LaCourse KD, Kempchinsky AG, Baryiames A, Barber B, Futran N, Houlton J, Sather C, Sicinska E, Taylor A, Minot SS, Johnston CD, Bullman S. 2022. Effect of the intratumoral microbiota on spatial and cellular heterogeneity in cancer. Nature 611:810–817. https://doi.org/10.1038/s41586-022-05435-0
62. Bourceau P, Geier B, Suerdieck V, Bien T, Soltwisch J, Dreisewerd K, Liebeke M. 2023. Visualization of metabolites and microbes at high spatial resolution using MALDI mass spectrometry imaging and *in situ* fluorescence labeling. Nat Protoc 18:3050–3079. https://doi.org/10.1038/s41596-023-00864-1
63. Yu T, Guo F, Yu Y, Sun T, Ma D, Han J, Qian Y, Kryczek I, Sun D, Nagarsheth N, Chen Y, Chen H, Hong J, Zou W, Fang J-Y. 2017. *Fusobacterium nucleatum* promotes chemoresistance to colorectal cancer by modulating autophagy. Cell 170:548–563. https://doi.org/10.1016/j.cell.2017.07.008
64. Gao Y, Bi D, Xie R, Li M, Guo J, Liu H, Guo X, Fang J, Ding T, Zhu H, Cao Y, Xing M, Zheng J, Xu Q, Xu Q, Wei Q, Qin H. 2021. *Fusobacterium nucleatum* enhances the efficacy of PD-L1 blockade in colorectal cancer. Signal Transduct Target Ther 6:398. https://doi.org/10.1038/s41392-021-00795-x
65. Chen T, Chen X, Zhang S, Zhu J, Tang B, Wang A, Dong L, Zhang Z, Yu C, Sun Y, Chi L, Chen H, Zhai S, Sun Y, Lan L, Zhang X, Xiao J, Bao Y, Wang Y, Zhang Z, Zhao W. 2021. The genome sequence archive family: toward explosive data growth and diverse data types. Genomics Proteomics Bioinformatics 19:578–583. https://doi.org/10.1016/j.gpb.2021.08.001
66. CNCB-NGDC Members and Partners. 2023. Database resources of the national genomics data center, China national center for bioinformation in 2023. Nucleic Acids Res 51:D18–D28. https://doi.org/10.1093/nar/gkac1073
67. Mirzayi C, Waldron L, Marques F. 2021. Reporting guidelines for human microbiome research: the STORMS checklist and analytical sample size flowchart. Nat Med:1–8. https://doi.org/10.52843/cassyni.hn51tm